

Elastic strain field due to an inclusion of a polyhedral shape with a non-uniform lattice misfit

A. V. Nenashev^{1,2} and A. V. Dvurechenskii^{1,2}

¹⁾ *Rzhanov Institute of Semiconductor Physics SB RAS, 630090 Novosibirsk, Russia*

²⁾ *Novosibirsk State University, 630090 Novosibirsk, Russia*

(Dated: 12 November 2018)

An analytical solution in a closed form is obtained for the three-dimensional elastic strain distribution in an unlimited medium containing an inclusion with a coordinate-dependent lattice mismatch (an eigenstrain). Quantum dots consisting of a solid solution with a spatially varying composition are examples of such inclusions. It is assumed that both the inclusion and the surrounding medium (the matrix) are elastically isotropic and have the same Young modulus and Poisson ratio. The inclusion shape is supposed to be an arbitrary polyhedron, and the coordinate dependence of the lattice misfit, with respect to the matrix, is assumed to be a polynomial of any degree. It is shown that, both inside and outside the inclusion, the strain tensor is expressed as a sum of contributions of all faces, edges and vertices of the inclusion. Each of these contributions, as a function of the observation point's coordinates, is a product of some polynomial and a simple analytical function, which is the solid angle subtended by the face from the observation point (for a contribution of a face), or the potential of the uniformly charged edge (for a contribution of an edge), or the distance from the vertex to the observation point (for a contribution of a vertex). The method of constructing the relevant polynomial functions is suggested. We also found out that similar expressions describe an electrostatic or gravitational potential, as well as its first and second derivatives, of a polyhedral body with a charge/mass density that depends on coordinates polynomially.

PACS numbers: 68.65.Hb, 46.25.-y

Keywords: quantum dot, eigenstrain, inclusion, analytical solution, potential

I. INTRODUCTION

Self-assembled quantum dots are inclusions of one semiconducting material within another material (a matrix). Due to different lattice constants of the two semiconductors, such structures possess built-in elastic strain, when grown coherently. The strain plays a key role both in the island self-assembly during heteroepitaxy,¹ and in electronic properties of quantum dots due to the strain effect on the carrier dispersion law.^{2,3} The strain is especially important in type-II heterostructures with quantum dots. For example, the electron localization in Ge/Si quantum dots occurs in potential wells formed in Si matrix near the Ge inclusion due to a spatially inhomogeneous strain.^{4,5} The knowledge of the spatial distribution of the strain induced by quantum dots is, therefore, important for the analysis of their electronic structure. It is natural in this context that many theoretical works on electronic properties of epitaxial quantum dots^{4,6-9} begin with considerations of the strain distribution.

There exist a few inclusion shapes, for which the problem of finding the strain distribution has an analytical solution in a closed form. Examples are two-dimensional problems of inclusions having polygonal shapes¹⁰⁻¹⁹ and some flat shapes with a curvilinear boundary;^{11,14} three-dimensional problems of ellipsoidal²⁰⁻²⁸ and polyhedral^{10,12,29-37} inclusions. An extensive list of bibliography on this issue can be found, for example, in Refs. 35, 36, 38, and 39. The present work is devoted to a three-dimensional polygonal inclusion. This choice is motivated by the facts that quantum

dots often have a faceted surface, and that a polyhedron is a convenient approximation to a body of an arbitrary shape.

The aim of the present study consists in finding an analytical expression (via elementary functions) for the three-dimensional distribution of the strain tensor $\varepsilon_{\alpha\beta}(x, y, z)$ within an inclusion (a quantum dot) and in the surrounding matrix, *taking into account spatial inhomogeneity of the misfit strain in the inclusion*. We will obtain, in this paper, an analytical solution for an arbitrary polyhedral-shaped inclusion with the lattice misfit $\varepsilon_0(x, y, z)$ described by any polynomial function of coordinates. The lattice misfit is defined as a relative deviation of the unstrained lattice constant a (which is determined by the composition of the material in a given point inside the inclusion) from the lattice constant of the environment a_0 :

$$\varepsilon_0(x, y, z) = \frac{a(x, y, z) - a_0}{a_0}. \quad (1)$$

The quantity ε_0 is often referred to as *eigenstrain*. The content of epitaxial quantum dots generally represents a solid solution with a composition smoothly varying in space.⁴⁰⁻⁴² This provides the motivation for considering a coordinate-dependent lattice misfit $\varepsilon_0(x, y, z)$.

Our analysis is based on the following simplifying assumptions. The elastic strain is considered in the continuous-medium, isotropic approximation. The lattice misfit is also isotropic. The strain is small. The inclusion and the surrounding matrix possess the same elastic properties, i. e., have the same values of Young

modulus and Poisson ratio. The matrix is spread to infinity in all directions.

Let us briefly survey what is currently known about analytical expressions for the strain induced by inclusions with a *spatially varied* lattice misfit. For ellipsoidal inclusions, such expressions have been known for several decades,^{22,24,28} and generalized for the case of anisotropic medium.²⁵ For a two-dimensional problem, where the inclusion shape and composition depend on two coordinates only, analytical answers were also obtained in the cases of linear,^{15,17} quadratic¹⁸ and, finally, arbitrary polynomial coordinate dependence of the lattice misfit,¹⁹ taking into account also elastic anisotropy and piezoeffect.

The problem of the *polyhedral* shaped inclusion with a constant lattice misfit was solved analytically in particular cases (a cuboid, a pyramid),^{12,29–32,34,35} as well as for the general polyhedron.^{10,33,36,37} Kuvshinov³⁶ showed that an analytical expression for the strain distribution should exist in the case of polynomial coordinate dependence of the lattice misfit, but he did not provide an explicit analytical formula. One can find, however, in the literature, the explicit solutions for a related problem—calculation of the Newtonian potential and its derivatives for a massive body of a polyhedral shape with an inhomogeneously distributed mass. This problem, being mathematically equivalent to the elasticity problem (see Section II), was solved however only in the simplest cases of linear^{43–47} and quadratic^{48–50} dependence of the mass density on coordinates. Thus, the task of the present paper has not been solved yet.

The present study is based on the approach developed in our previous work, Ref. 37. In this work, the strain due to a polyhedral inclusion with a *constant* lattice misfit is shown to be a sum of contributions of *faces* and *edges* of the polyhedron. A contribution of a face is proportional to the solid angle subtended by this face. (The role of solid angles in calculating the potential and the strain is mentioned also in Refs. 31, 36, and 51.) A contribution of an edge is proportional to the potential induced of this edge, as if it were uniformly charged (see also Ref. 51). In the present paper, this result is generalized to the case of a non-uniform lattice misfit in the following way. At first, the coefficients of proportionality at face and edge contributions become polynomial functions of coordinates of the observation point. At second, the contributions of *vertices* of the polyhedron to the strain tensor are also introduced; for each vertex, its contribution is equal to the product of some polynomial function of coordinates and the distance between this vertex and the observation point. We prove that such modification of the results of Ref. 37 indeed provides a solution for the problem of the present work, and suggest an algorithm for finding the coefficients of all needed polynomials.

Before proceeding to the development of the solution, let us introduce some notations. The coordinate-dependent lattice misfit $\varepsilon_0(\mathbf{r})$ defined by Eq. (1) can be

represented as

$$\varepsilon_0(\mathbf{r}) = \begin{cases} f(\mathbf{r}) & \text{if } \mathbf{r} \text{ is inside the inclusion,} \\ 0 & \text{if } \mathbf{r} \text{ is outside the inclusion,} \end{cases} \quad (2)$$

with $f(\mathbf{r})$ being a polynomial function of coordinates x, y, z of some degree N :

$$f(x, y, z) = \sum_{\substack{m, n, p \\ m+n+p \leq N}} C_{mnp} x^m y^n z^p. \quad (3)$$

Sometimes it is convenient to represent the function $\varepsilon_0(\mathbf{r})$ as

$$\varepsilon_0(\mathbf{r}) = f(\mathbf{r}) \chi(\mathbf{r}), \quad (4)$$

where $\chi(\mathbf{r})$ is the characteristic function that determines whether the point \mathbf{r} belongs to the inclusion:

$$\chi(\mathbf{r}) = \begin{cases} 1 & \text{if } \mathbf{r} \text{ is inside the inclusion,} \\ 0 & \text{otherwise.} \end{cases} \quad (5)$$

Our goal is to calculate the strain tensor $\varepsilon_{\alpha\beta}$ at an arbitrary point $\mathbf{R} = (X, Y, Z)$:

$$\varepsilon_{\alpha\beta}(\mathbf{R}) = ? \quad (6)$$

Also, as we will see in Section II, an important function for our consideration is the electrostatic potential $\varphi(\mathbf{r})$ that is produced by the charge distribution defined by the function $\varepsilon_0(\mathbf{r})$. More formally, $\varphi(\mathbf{r})$ is the solution of Poisson equation

$$\Delta\varphi(\mathbf{r}) = -4\pi\varepsilon_0(\mathbf{r}), \quad (7)$$

which vanishes at infinity. We will also represent the analytical expressions for the potential $\varphi(\mathbf{r})$ and its first and second derivatives.

This paper is organized as follows. The connection between the strain $\varepsilon_{\alpha\beta}$ and the potential φ is explained in Section II. In Sections III and IV we will express the potential φ in terms of more simple quantities—four kinds of “primitives” introduced in Section IV. They can be considered as potentials induced by a charge inhomogeneously distributed over the inclusion, or over some its face, or over some its edge, or by a double layer inhomogeneously covering one of the inclusion faces. Then, in Sections V and VI we will show how to find analytical expressions for the “primitives”. All these results are summed up in Section VII, yielding the final analytical formula for the strain distribution $\varepsilon_{\alpha\beta}(\mathbf{R})$ (Subsection VII A) and the algorithm for finding the polynomial coefficients contributing to this formula (Subsection VII B). Analytical results for the potential φ and its derivatives are also supplied. Section VIII provides some examples of applying the general answer to particular cases. Concluding remarks are presented in Section IX.

II. ELASTIC-ELECTROSTATIC ANALOGY

The displacement field $\mathbf{u}(\mathbf{r})$ in an isotropic elastic medium caused by a point-like isotropic inclusion (put at $\mathbf{r} = 0$) looks just like the electric field of a point charge:

$$\mathbf{u}(\mathbf{r}) \propto \frac{\mathbf{r}}{r^3}. \quad (8)$$

This simple fact provides a basis for the analogy between the problems of electrostatics and of elasticity theory. More precisely, if the elastic medium is infinite and isotropic, and its Young module and Poisson ratio are constant throughout the whole space, then the displacement induced by the eigenstrain distribution $\varepsilon_0(\mathbf{r})$ can be expressed as follows^{52,53}:

$$\mathbf{u}(\mathbf{r}) = -\Lambda \frac{\partial \varphi(\mathbf{r})}{\partial \mathbf{r}}, \quad (9)$$

where $\varphi(\mathbf{r})$ is the potential defined by Eq. (7), and the coefficient Λ is related to the Poisson ratio ν :

$$\Lambda = \frac{1}{4\pi} \frac{1 + \nu}{1 - \nu}. \quad (10)$$

Since the strain tensor $\varepsilon_{\alpha\beta}$ is defined via derivatives of the displacement,

$$\varepsilon_{\alpha\beta}(\mathbf{r}) = \frac{1}{2} \left(\frac{\partial u_\alpha}{\partial r_\beta} + \frac{\partial u_\beta}{\partial r_\alpha} \right) - \delta_{\alpha\beta} \varepsilon_0(\mathbf{r}), \quad (11)$$

then it is a combination of *second* derivatives of φ :^{37,53}

$$\varepsilon_{\alpha\beta}(\mathbf{r}) = -\Lambda \frac{\partial^2 \varphi(\mathbf{r})}{\partial r_\alpha \partial r_\beta} - \delta_{\alpha\beta} \varepsilon_0(\mathbf{r}). \quad (12)$$

Here $\delta_{\alpha\beta}$ is the Kronecker delta.

Obviously, the potential φ has an integral representation:

$$\varphi(\mathbf{R}) = \iiint \varepsilon_0(\mathbf{r}) \frac{d^3 r}{|\mathbf{r} - \mathbf{R}|} \equiv \iiint_{\text{inclusion}} f(\mathbf{r}) \frac{d^3 r}{|\mathbf{r} - \mathbf{R}|}, \quad (13)$$

as well as its first and second derivatives:

$$\frac{\partial \varphi(\mathbf{R})}{\partial \mathbf{R}} = \iiint \frac{\partial \varepsilon_0(\mathbf{r})}{\partial \mathbf{r}} \frac{d^3 r}{|\mathbf{r} - \mathbf{R}|}, \quad (14)$$

$$\frac{\partial^2 \varphi(\mathbf{R})}{\partial R_\alpha \partial R_\beta} = \iiint \frac{\partial^2 \varepsilon_0(\mathbf{r})}{\partial r_\alpha \partial r_\beta} \frac{d^3 r}{|\mathbf{r} - \mathbf{R}|}. \quad (15)$$

(Triple integrals without specification of the domain are assumed to be over the whole space.) The latter equation provides also an integral representation for the strain tensor, by virtue of Eq. (12). It is important to note that integrals (13)–(15) were extensively studied in the context of geophysical^{43–46,48–50,54–61} and astronomy/spacecraft^{47,51,62,63} problems. But, as mentioned in Introduction, fully analytical expressions for polyhedral bodies were obtained only when the density $f(\mathbf{r})$ is a constant ($N=0$), a linear ($N=1$) or a quadratic ($N=2$) function of coordinates.

In the next Section, we transform these integrals into a form more convenient for further analysis.

III. FROM POLYNOMIALS TO MONOMIALS

It is easier to deal with potentials induced by charge density distributions of the following form:

$$\rho_{mnp}(\mathbf{r}; \mathbf{R}) = (x - X)^m (y - Y)^n (z - Z)^p \chi(\mathbf{r}), \quad (16)$$

where m, n, p are non-negative integer numbers, and the characteristic function $\chi(\mathbf{r})$ is defined in Eq. (5). One can expand the “actual” density $\varepsilon_0(\mathbf{r})$ into a series of terms ρ_{mnp} :

$$\varepsilon_0(\mathbf{r}) = \sum_{\substack{m,n,p \\ m+n+p \leq N}} \tilde{C}_{mnp}(\mathbf{R}) \rho_{mnp}(\mathbf{r}; \mathbf{R}). \quad (17)$$

Each of the coefficients \tilde{C}_{mnp} is a polynomial of X, Y, Z of degree $N - m - n - p$. The explicit expression for polynomials $\tilde{C}_{mnp}(\mathbf{R})$ can be obtained by substituting Eqs. (2), (3) and (16) into Eq. (17), that leads to the identity

$$\begin{aligned} & \sum_{m,n,p} C_{mnp} x^m y^n z^p \\ &= \sum_{m,n,p} \tilde{C}_{mnp}(\mathbf{R}) (x - X)^m (y - Y)^n (z - Z)^p, \end{aligned} \quad (18)$$

whence

$$\begin{aligned} \tilde{C}_{mnp}(\mathbf{R}) &= \\ & \sum_{\substack{m' \geq m \\ n' \geq n \\ p' \geq p}} C_{m'n'p'} \binom{m'}{m} \binom{n'}{n} \binom{p'}{p} X^{m'-m} Y^{n'-n} Z^{p'-p}, \end{aligned} \quad (19)$$

where symbols $\binom{m'}{m}$ are binomial coefficients.

Substituting the expansion (17) into Eqs. (13)–(15), one can get similar expansions for the potential $\varphi(\mathbf{R})$ and its derivatives:

$$\varphi(\mathbf{R}) = \sum_{m,n,p} \tilde{C}_{mnp}(\mathbf{R}) \varphi_{mnp}(\mathbf{R}), \quad (20)$$

$$\frac{\partial \varphi(\mathbf{R})}{\partial R_\alpha} = \sum_{m,n,p} \tilde{C}_{mnp}(\mathbf{R}) \varphi_{,\alpha}^{(mnp)}(\mathbf{R}), \quad (21)$$

$$\frac{\partial^2 \varphi(\mathbf{R})}{\partial R_\alpha \partial R_\beta} = \sum_{m,n,p} \tilde{C}_{mnp}(\mathbf{R}) \varphi_{,\alpha\beta}^{(mnp)}(\mathbf{R}), \quad (22)$$

where symbols φ_{mnp} , $\varphi_{,\alpha}^{(mnp)}$, $\varphi_{,\alpha\beta}^{(mnp)}$ denote potentials and their derivatives induced by “monomial” charge distributions ρ_{mnp} defined in Eq. (16):

$$\varphi_{mnp}(\mathbf{R}) = \iiint (x - X)^m (y - Y)^n (z - Z)^p \chi(\mathbf{r}) \frac{d^3 r}{|\mathbf{r} - \mathbf{R}|}, \quad (23)$$

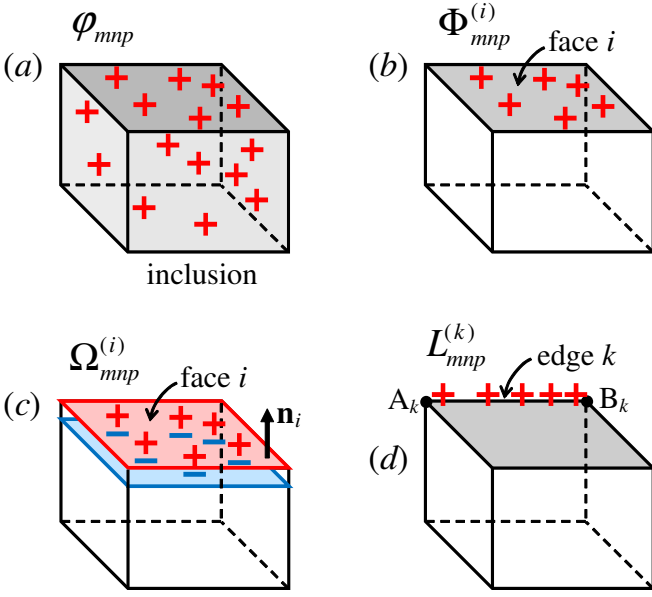


FIG. 1. The primitives φ_{mnp} , $\Phi_{mnp}^{(i)}$, $\Omega_{mnp}^{(i)}$, $L_{mnp}^{(k)}$ as potentials induced at point $\mathbf{R} = (X, Y, Z)$ by the following inhomogeneous charge distributions as functions of coordinates x, y, z : (a) by a charged inclusion with *volume* density $(x - X)^m(y - Y)^n(z - Z)^p$; (b) by charged *ith* face with *surface* charge density $(x - X)^m(y - Y)^n(z - Z)^p$; (c) by *ith* face covered by a doubly charged layer with *surface density of dipole moment* $(x - X)^m(y - Y)^n(z - Z)^p$; (d) by *kth* edge with *linear* charge density $(x - X)^m(y - Y)^n(z - Z)^p$.

$$\begin{aligned} & \varphi_{,\alpha}^{(mnp)}(\mathbf{R}) \\ &= \iiint \frac{\partial [(x - X)^m(y - Y)^n(z - Z)^p \chi(\mathbf{r})]}{\partial r_\alpha} \frac{d^3r}{|\mathbf{r} - \mathbf{R}|}, \end{aligned} \quad (24)$$

$$\begin{aligned} & \varphi_{,\alpha\beta}^{(mnp)}(\mathbf{R}) \\ &= \iiint \frac{\partial^2 [(x - X)^m(y - Y)^n(z - Z)^p \chi(\mathbf{r})]}{\partial r_\alpha \partial r_\beta} \frac{d^3r}{|\mathbf{r} - \mathbf{R}|}. \end{aligned} \quad (25)$$

IV. FOUR PRIMITIVES φ_{mnp} , $\Phi_{mnp}^{(i)}$, $\Omega_{mnp}^{(i)}$, $L_{mnp}^{(k)}$

We will consider four types of “primitive constituents” of the potential and its derivatives. The first one, φ_{mnp} , is the potential provided at point $\mathbf{R} = (X, Y, Z)$ by the charged inclusion (Fig. 1a) with the charge density depending on coordinates x, y, z as $(x - X)^m(y - Y)^n(z - Z)^p$:

$$\varphi_{mnp}(\mathbf{R}) = \iiint_{\text{inclusion}} \frac{(x - X)^m(y - Y)^n(z - Z)^p}{|\mathbf{r} - \mathbf{R}|} dV. \quad (26)$$

This expression is just a different form of Eq. (23).

The second primitive, $\Phi_{mnp}^{(i)}$, is the potential of one of the inclusion faces (number i) charged with surface charge density $(x - X)^m(y - Y)^n(z - Z)^p$ (Fig. 1b):

$$\Phi_{mnp}^{(i)}(\mathbf{R}) = \iint_{\text{face } i} \frac{(x - X)^m(y - Y)^n(z - Z)^p}{|\mathbf{r} - \mathbf{R}|} dS. \quad (27)$$

The third primitive, $\Omega_{mnp}^{(i)}$, is the potential of one of i th face covered with a thin dipole layer with dipole moment density $(x - X)^m(y - Y)^n(z - Z)^p$:

$$\Omega_{mnp}^{(i)}(\mathbf{R}) = \iint_{\text{face } i} (x - X)^m(y - Y)^n(z - Z)^p \frac{(\mathbf{R} - \mathbf{r}) \cdot \mathbf{n}_i}{|\mathbf{r} - \mathbf{R}|^3} dS, \quad (28)$$

where \mathbf{n}_i is the unit normal vector to i th face, directed outside the inclusion (see Fig. 1c).

And the fourth one, $L_{mnp}^{(k)}$, is the potential due to k th edge of the inclusion, being charged with linear charge density $(x - X)^m(y - Y)^n(z - Z)^p$:

$$L_{mnp}^{(k)}(\mathbf{R}) = \int_{A_k}^{B_k} \frac{(x - X)^m(y - Y)^n(z - Z)^p}{|\mathbf{r} - \mathbf{R}|} dl, \quad (29)$$

where A_k and B_k are two ends of the k th edge (Fig. 1d).

Significance of these primitives for our study consists in the fact that the quantities φ_{mnp} , $\varphi_{,\alpha}^{(mnp)}$, $\varphi_{,\alpha\beta}^{(mnp)}$ that appear in Eqs. (20)–(22) can be expressed through them. As shown in Appendix A, $\varphi_{,\alpha}^{(mnp)}$ has the representation

$$\varphi_{,\alpha}^{(mnp)} = \varphi_{(mnp),\alpha} - \sum_i n_{i\alpha} \Phi_{mnp}^{(i)}, \quad (30)$$

where $\varphi_{(mnp),\alpha}$ is the following volume integral:

$$\begin{aligned} & \varphi_{(mnp),\alpha} \\ &= \iiint \frac{\partial [(x - X)^m(y - Y)^n(z - Z)^p]}{\partial r_\alpha} \chi(\mathbf{r}) \frac{d^3r}{|\mathbf{r} - \mathbf{R}|}. \end{aligned} \quad (31)$$

One can conclude from comparison between Eqs. (23) and (31) that

$$\varphi_{(mnp),x} = m \varphi_{m-1,n,p}, \quad (32a)$$

$$\varphi_{(mnp),y} = n \varphi_{m,n-1,p}, \quad (32b)$$

$$\varphi_{(mnp),z} = p \varphi_{m,n,p-1}. \quad (32c)$$

In order to write down a representation of $\varphi_{,\alpha\beta}^{(mnp)}$ in terms of the primitives, let us introduce, for each face i and each edge k adjacent to this face, a unit vector \mathbf{b}_{ik} directed perpendicularly to k th edge, along i th face and out of this face (see Fig. 2). Also, for each edge k , we define a tensor $\lambda_{\alpha\beta}^{(k)}$ as follows:³⁷

$$\lambda_{\alpha\beta}^{(k)} = n_{i_1\alpha} b_{i_1k\beta} + n_{i_2\alpha} b_{i_2k\beta}, \quad (33)$$

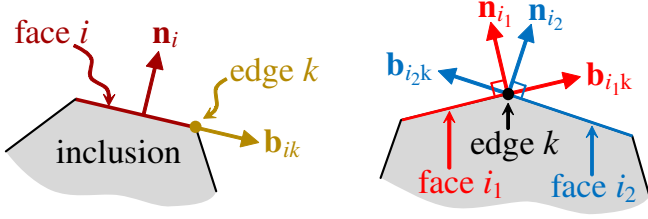


FIG. 2. Illustration of the definition of unit vectors \mathbf{n}_i and \mathbf{b}_{ik} (left); four unit vectors contributing to the definition (33) of the tensor $\lambda_{\alpha\beta}^{(k)}$ (right).

where i_1 and i_2 are numbers of the two faces, which intersect at k th edge, as illustrated in Fig. 2. Then, the quantity $\varphi_{,\alpha\beta}^{(mnp)}$ takes the following representation (for derivation, see Appendix A):

$$\begin{aligned} \varphi_{,\alpha\beta}^{(mnp)} &= \varphi_{(mnp),\alpha\beta} \\ &+ \sum_{\substack{i \\ (\text{faces})}} \left(-n_{i\alpha} \Phi_{(mnp),\beta}^{(i)} - n_{i\beta} \Phi_{(mnp),\alpha}^{(i)} + n_{i\alpha} n_{i\beta} n_{i\gamma} \Phi_{(mnp),\gamma}^{(i)} \right) \\ &+ \sum_{\substack{i \\ (\text{faces})}} n_{i\alpha} n_{i\beta} \Omega_{mnp}^{(i)} + \sum_{\substack{k \\ (\text{edges})}} \lambda_{\alpha\beta}^{(k)} L_{mnp}^{(k)}, \end{aligned} \quad (34)$$

where $\varphi_{(mnp),\alpha\beta}$ and $\Phi_{(mnp),\alpha}^{(i)}$ are defined as follows:

$$\begin{aligned} \varphi_{(mnp),\alpha\beta} &= \iiint \frac{\partial^2 [(x-X)^m (y-Y)^n (z-Z)^p]}{\partial r_\alpha \partial r_\beta} \chi(\mathbf{r}) \frac{d^3 r}{|\mathbf{r}-\mathbf{R}|}, \end{aligned} \quad (35)$$

$$\begin{aligned} \Phi_{(mnp),\alpha}^{(i)} &= \iint_{\text{face } i} \frac{\partial [(x-X)^m (y-Y)^n (z-Z)^p]}{\partial r_\alpha} \frac{dS}{|\mathbf{r}-\mathbf{R}|}. \end{aligned} \quad (36)$$

From the comparison between Eqs. (23) and (35) it is easy to express the quantities $\varphi_{(mnp),\alpha\beta}$ through primitives $\varphi_{m'n'p'}$:

$$\varphi_{(mnp),xx} = m(m-1) \varphi_{m-2,n,p}, \quad (37a)$$

$$\varphi_{(mnp),xy} = mn \varphi_{m-1,n-1,p}, \quad (37b)$$

and so on. Similarly, the comparison between Eqs. (27) and (36) provides the following relations:

$$\Phi_{(mnp),x}^{(i)} = m \Phi_{m-1,n,p}^{(i)}, \quad (38a)$$

$$\Phi_{(mnp),y}^{(i)} = n \Phi_{m,n-1,p}^{(i)}, \quad (38b)$$

$$\Phi_{(mnp),z}^{(i)} = p \Phi_{m,n,p-1}^{(i)}. \quad (38c)$$

In the simplest case of $m = n = p = 0$, Eq. (34) is simplified to^{37,51}

$$\varphi_{,\alpha\beta}^{(000)} = \sum_i n_{i\alpha} n_{i\beta} \Omega_{000}^{(i)} + \sum_k \lambda_{\alpha\beta}^{(k)} L_{000}^{(k)}. \quad (39)$$

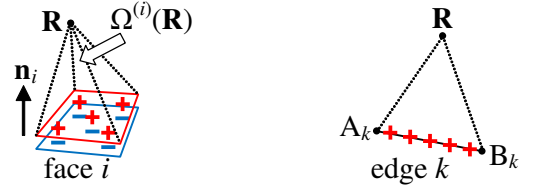


FIG. 3. The meaning of the quantity $\Omega^{(i)}(\mathbf{R})$ as a potential due to a dipole layer at point \mathbf{R} and as a solid angle (left); the quantity $L^{(k)}(\mathbf{R})$ as a potential of a uniformly charged rod at point \mathbf{R} (right).

The primitives $\Omega_{000}^{(i)}$ and $L_{000}^{(k)}$ have simple physical and geometrical meanings and well-known analytical representations. Below we will drop the index “000” at them:

$$\Omega_{000}^{(i)} \equiv \Omega^{(i)}, \quad L_{000}^{(k)} \equiv L^{(k)}. \quad (40)$$

The quantity $\Omega^{(i)}(\mathbf{R})$ is the potential at point \mathbf{R} due to a flat polygon (i th face of the inclusion) covered by a uniform dipole layer of unit density, see Fig. 3. The absolute value of $\Omega^{(i)}(\mathbf{R})$ is equal to the solid angle, at which the polygon is seen from the point \mathbf{R} .^{64,65} And the sign of $\Omega^{(i)}(\mathbf{R})$ is positive if the normal vector \mathbf{n}_i is directed towards the point \mathbf{R} , and negative otherwise. There are several recipes in the literature, how to calculate such solid angles analytically.^{51,66,67}

It is important to note that the characteristic function of the inclusion $\chi(\mathbf{r})$ can be expressed in terms of solid angles:

$$\chi(\mathbf{r}) = -\frac{1}{4\pi} \sum_i \Omega^{(i)}(\mathbf{r}). \quad (41)$$

Indeed, if the point \mathbf{r} is inside the inclusion, then each of the quantities $\Omega^{(i)}(\mathbf{r})$ is negative, so their sum is equal to -4π (the total solid angle). When \mathbf{r} is outside the inclusion, then some of quantities $\Omega^{(i)}(\mathbf{r})$ are positive, and some are negative; moreover, the sum of negative Ω 's exactly compensates the sum of positive ones. From Eqs. (4) and (41) one can get a representation of the lattice misfit ε_0 :

$$\varepsilon_0(\mathbf{r}) = -\frac{f(\mathbf{r})}{4\pi} \sum_i \Omega^{(i)}(\mathbf{r}). \quad (42)$$

The quantity $L^{(k)}(\mathbf{R})$ is the potential at point \mathbf{R} of a thin, uniformly charged rod (k th edge) with unit linear charge density, see Fig. 3. Elementary integration provides the following expression for $L^{(k)}$.^{37,51}

$$L^{(k)}(\mathbf{R}) = \log \frac{RA_k + RB_k + A_k B_k}{RA_k + RB_k - A_k B_k}, \quad (43)$$

where RA_k , RB_k and $A_k B_k$ are distances between the point \mathbf{R} and two end points A_k and B_k of k th edge.

The main results of this Section are equations (30), (32), (34), (37), (38), which (together with the results of the previous sections) allow one to express the strain tensor, the potential and derivatives of the potential via four kinds of primitives.

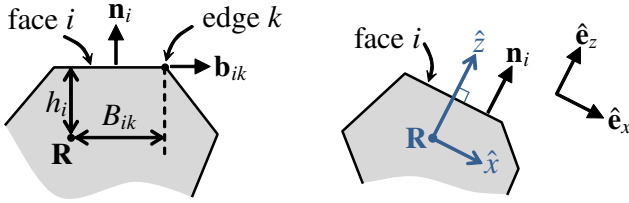


FIG. 4. The meaning of the quantities h_i and B_{ik} defined by Eqs. (44) and (45) (left); the “tilted” frame associated with i th face(right).

V. REDUCING PRIMITIVES φ_{mnp} , $\Phi_{mnp}^{(i)}$, $\Omega_{mnp}^{(i)}$ TO SOLID ANGLES AND LINE INTEGRALS

In this Section, we will demonstrate how to simplify the functions $\varphi_{mnp}(\mathbf{R})$, $\Phi_{mnp}^{(i)}(\mathbf{R})$ and $\Omega_{mnp}^{(i)}(\mathbf{R})$ by reducing them to the solid angles $\Omega^{(i)}(\mathbf{R})$ and to some line integrals along the edges of the polyhedron. For this purpose, we will use two linear functions of \mathbf{R} : $h_i(\mathbf{R})$ and $B_{ik}(\mathbf{R})$, whose meaning is illustrated in Fig. 4. The function $h_i(\mathbf{R})$ is defined as follows:

$$h_i(\mathbf{R}) = (\mathbf{r}_i - \mathbf{R}) \cdot \mathbf{n}_i, \quad (44)$$

where \mathbf{r}_i is a radius vector of some point on i th face. (The value of h_i does not depend on the choice of the point \mathbf{r}_i , because the vector \mathbf{n}_i is orthogonal to the face.) The absolute value of h_i has the meaning of the distance from \mathbf{R} to the plane of i th face.

The function $B_{ik}(\mathbf{R})$ has the following definition:

$$B_{ik}(\mathbf{R}) = (\mathbf{r}_k - \mathbf{R}) \cdot \mathbf{b}_{ik}, \quad (45)$$

where \mathbf{r}_k is a radius vector of some point on k th edge. Since the vector \mathbf{b}_{ik} is orthogonal to the edge, the choice of the point \mathbf{r}_k does not matter. The absolute value of B_{ik} is the distance between the projection of the point \mathbf{R} to i th face and the line of k th edge, as illustrated in Fig. 4.

We start from the usual recipe of reducing volume integrals to surface integrals. Applying Gauss’s theorem to the vector

$$\mathbf{F}(\mathbf{r}) = \frac{\mathbf{r} - \mathbf{R}}{|\mathbf{r} - \mathbf{R}|} (x - X)^m (y - Y)^n (z - Z)^p, \quad (46)$$

one can reduce the volume integral φ_{mnp} to integrals over inclusion faces. The details of the derivation can be found in Appendix B. The answer reads:

$$\varphi_{mnp} = \frac{1}{m + n + p + 2} \sum_i h_i \Phi_{mnp}^{(i)}. \quad (47)$$

Now let us consider the primitives $\Phi_{mnp}^{(i)}$ and $\Omega_{mnp}^{(i)}$ for one of the faces (say, i th face). It is convenient to choose temporarily a system of coordinates $\hat{x}, \hat{y}, \hat{z}$ related to i th face, so that the axis \hat{z} is perpendicular to this face. For that, we choose three mutually orthogonal normal vectors

$\hat{\mathbf{e}}_x, \hat{\mathbf{e}}_y, \hat{\mathbf{e}}_z$ such that $\hat{\mathbf{e}}_z = \mathbf{n}_i$, and define the coordinates $\hat{x}, \hat{y}, \hat{z}$ as follows:

$$\hat{x} = (\mathbf{r} - \mathbf{R}) \cdot \hat{\mathbf{e}}_x, \quad \hat{y} = (\mathbf{r} - \mathbf{R}) \cdot \hat{\mathbf{e}}_y, \quad (48a)$$

$$\hat{z} = (\mathbf{r} - \mathbf{R}) \cdot \hat{\mathbf{e}}_z \equiv (\mathbf{r} - \mathbf{R}) \cdot \mathbf{n}_i \quad (48b)$$

(see Fig. 4). Then, let us define quantities $\hat{\Phi}_{mnp}^{(i)}$, $\hat{\Omega}_{mnp}^{(i)}$ and $\hat{L}_{mnp}^{(k)}$ similar to the primitives $\Phi_{mnp}^{(i)}$, $\Omega_{mnp}^{(i)}$, $L_{mnp}^{(k)}$ but related to the “tilted” axes $\hat{x}, \hat{y}, \hat{z}$:

$$\hat{\Phi}_{mnp}^{(i)} = \iint_{\text{face } i} \frac{\hat{x}^m \hat{y}^n \hat{z}^p}{\hat{r}} dS, \quad (49a)$$

$$\hat{\Omega}_{mnp}^{(i)} = - \iint_{\text{face } i} \hat{x}^m \hat{y}^n \hat{z}^p \frac{\hat{z}}{\hat{r}^3} dS, \quad (49b)$$

$$\hat{L}_{mnp}^{(k)} = \int_{A_k}^{B_k} \frac{\hat{x}^m \hat{y}^n \hat{z}^p}{\hat{r}} dl, \quad (49c)$$

where $\hat{r} = (\hat{x}^2 + \hat{y}^2 + \hat{z}^2)^{1/2} = |\mathbf{r} - \mathbf{R}|$. (The considered edges are those that surround i th face.) Obviously, the “untilted” quantities are linear combinations of “tilted” ones:

$$\Phi_{mnp}^{(i)} = \sum_{m', n', p'} T_{mnp}^{m' n' p'} \hat{\Phi}_{m' n' p'}^{(i)}, \quad (50a)$$

$$\Omega_{mnp}^{(i)} = \sum_{m', n', p'} T_{mnp}^{m' n' p'} \hat{\Omega}_{m' n' p'}^{(i)}, \quad (50b)$$

with coefficients $T_{mnp}^{m' n' p'}$ defined by the identity

$$(x - X)^m (y - Y)^n (z - Z)^p = \sum_{m', n', p'} T_{mnp}^{m' n' p'} \hat{x}^{m'} \hat{y}^{n'} \hat{z}^{p'}. \quad (51)$$

Note that, at $m = n = p = 0$, the quantities $\Phi_{mnp}^{(i)}$, $\Omega_{mnp}^{(i)}$ and $L_{mnp}^{(k)}$ are invariant with respect to the choice of coordinates. Consequently,

$$\hat{\Phi}_{000}^{(i)} = \Phi_{000}^{(i)}, \quad (52a)$$

$$\hat{\Omega}_{000}^{(i)} = \Omega_{000}^{(i)} = \Omega^{(i)}, \quad (52b)$$

$$\hat{L}_{000}^{(k)} = L_{000}^{(k)} = L^{(k)}. \quad (52c)$$

Then, it is easy to get rid of the index p in $\hat{\Phi}_{mnp}^{(i)}$ and $\hat{\Omega}_{mnp}^{(i)}$. One can see from Eqs. (44) and (48b) that i th face lies in a plane of constant coordinate $\hat{z} = h_i$. One can therefore take the factor \hat{z}^p outside the integral sign in Eqs. (49a), (49b), what gives

$$\hat{\Phi}_{mnp}^{(i)} = h_i^p \hat{\Phi}_{mn0}^{(i)}, \quad \hat{\Omega}_{mnp}^{(i)} = h_i^p \hat{\Omega}_{mn0}^{(i)}. \quad (53)$$

Applying the planar variant of Gauss’s theorem to the vector $(G_{\hat{x}}, G_{\hat{y}})$ defined as

$$G_{\hat{x}}(\hat{x}, \hat{y}) = \frac{\hat{x}^{m+1} \hat{y}^n}{\hat{r}}, \quad G_{\hat{y}}(\hat{x}, \hat{y}) = \frac{\hat{x}^m \hat{y}^{n+1}}{\hat{r}}, \quad (54)$$

one can reduce the surface integral $\hat{\Phi}_{mn0}^{(i)}$ to the quantity $\hat{\Omega}_{mn0}^{(i)}$ and line integrals $\hat{L}_{mn0}^{(k)}$. The details of the calculation can be found in Appendix C, and the following result was obtained:

$$\hat{\Phi}_{mn0}^{(i)} = \frac{h_i}{m+n+1} \hat{\Omega}_{mn0}^{(i)} + \sum_k \frac{B_{ik}}{m+n+1} \hat{L}_{mn0}^{(k)}. \quad (55)$$

Here and below in this section, the index k runs over edges adjacent to i th face.

The next step is decreasing the index n at $\hat{\Omega}_{mn0}^{(i)}$. If $n \geq 2$, one can apply the following relation derived in Appendix D,

$$\begin{aligned} \hat{\Omega}_{mn0}^{(i)} = & -\hat{\Omega}_{m+2,n-2,0}^{(i)} - \frac{m+n}{m+n-1} h_i^2 \hat{\Omega}_{m,n-2,0}^{(i)} \\ & - h_i \sum_k \frac{B_{ik}}{m+n-1} \hat{L}_{m,n-2,0}^{(k)}. \end{aligned} \quad (56)$$

This recursive relation makes it possible to lower the second index at Ω down to $n = 1$ or $n = 0$.

In the case of $n = 1$, the expression for $\hat{\Omega}_{m10}^{(i)}$ can be simplified by direct integration over \hat{y} (see details in Appendix E), yielding

$$\hat{\Omega}_{m10}^{(i)} = h_i \sum_k (\mathbf{b}_{ik} \cdot \hat{\mathbf{e}}_y) \hat{L}_{m00}^{(k)}. \quad (57)$$

The last case to consider is that of $n = 0$. If $m \geq 2$, one can reduce m by two as follows:

$$\hat{\Omega}_{m00}^{(i)} = -h_i^2 \hat{\Omega}_{m-2,0,0}^{(i)} - h_i \sum_k (\mathbf{b}_{ik} \cdot \hat{\mathbf{e}}_y) \hat{L}_{m-2,1,0}^{(k)}. \quad (58)$$

This relation is derived in Appendix F. Applying Eq. (58) repeatedly, one arrives finally at $\hat{\Omega}_{100}^{(i)}$ or $\hat{\Omega}_{000}^{(i)} \equiv \Omega^{(i)}$ plus line integrals.

Finally, the value of $\hat{\Omega}_{100}^{(i)}$ can be found in full analogy with Eq. (57):

$$\hat{\Omega}_{100}^{(i)} = h_i \sum_k (\mathbf{b}_{ik} \cdot \hat{\mathbf{e}}_x) L^{(k)}. \quad (59)$$

Thus, we have seen in this section that any of quantities φ_{mnp} , $\Phi_{mnp}^{(i)}$, $\Omega_{mnp}^{(i)}$ can be reduced to line integrals over inclusion edges and/or to solid angles $\Omega^{(i)}$. A simple but not so trivial example of such reducing will be considered in Subsection V A. Then, in Section VI, we will know how to evaluate the line integrals.

A. Example: evaluation of $\Omega_{001}^{(i)}$

Here we will apply the above-formulated considerations to finding an analytical expression for the quantity $\Omega_{001}^{(i)}$. The first step is choosing the “tilted” frame associated with i th face of the polyhedron, i. e., choosing three mutually orthogonal unit vectors $\hat{\mathbf{e}}_x$, $\hat{\mathbf{e}}_y$, $\hat{\mathbf{e}}_z$ along



FIG. 5. Unit vectors $\hat{\mathbf{e}}_z$ and $\hat{\mathbf{e}}_x$ as defined by Eqs. (60) and (61).

the axes of the “tilted” frame. The vector $\hat{\mathbf{e}}_z$ should be orthogonal to i th face:

$$\hat{\mathbf{e}}_z = \mathbf{n}_i. \quad (60)$$

We choose the vector $\hat{\mathbf{e}}_x$ in the plane spanned onto \mathbf{e}_z and $\hat{\mathbf{e}}_z$ (see Fig. 5):

$$\hat{\mathbf{e}}_x = \frac{\mathbf{e}_z - \hat{\mathbf{e}}_z \cos \theta}{\sin \theta}, \quad (61)$$

where θ is the angle between \mathbf{e}_z and $\hat{\mathbf{e}}_z$:

$$\cos \theta = \mathbf{e}_z \cdot \hat{\mathbf{e}}_z \equiv \mathbf{e}_z \cdot \mathbf{n}_i \equiv n_{iz}. \quad (62)$$

And the vector $\hat{\mathbf{e}}_y$ is to be orthogonal to $\hat{\mathbf{e}}_x$ and $\hat{\mathbf{e}}_z$.

Then, according to Eq. (50b), $\Omega_{001}^{(i)}$ is a linear combination of the “tilted” quantities $\hat{\Omega}_{100}^{(i)}$, $\hat{\Omega}_{010}^{(i)}$ and $\hat{\Omega}_{001}^{(i)}$, taken with their respective coefficients T_{001}^{100} , T_{001}^{010} and T_{001}^{001} . In order to find these coefficients from Eq. (51), one should represent the value of $z - Z$ via the “tilted” coordinates \hat{x} , \hat{y} , \hat{z} :

$$z - Z = (\mathbf{r} - \mathbf{R}) \cdot \mathbf{e}_z = (\hat{x} \hat{\mathbf{e}}_x + \hat{y} \hat{\mathbf{e}}_y + \hat{z} \hat{\mathbf{e}}_z) \cdot \mathbf{e}_z = \hat{x} \sin \theta + \hat{z} \cos \theta; \quad (63)$$

whence, $T_{001}^{100} = \sin \theta$, $T_{001}^{010} = 0$, and $T_{001}^{001} = \cos \theta$. Therefore

$$\Omega_{001}^{(i)} = \hat{\Omega}_{100}^{(i)} \sin \theta + \hat{\Omega}_{001}^{(i)} \cos \theta. \quad (64)$$

Then one can evaluate the quantity $\hat{\Omega}_{100}^{(i)}$ using Eq. (59), where scalar products $\mathbf{b}_{ik} \cdot \hat{\mathbf{e}}_x$ can be found from Eq. (61) taking into account that the vector \mathbf{b}_{ik} is orthogonal to $\hat{\mathbf{e}}_z \equiv \mathbf{n}_i$:

$$\mathbf{b}_{ik} \cdot \hat{\mathbf{e}}_x = \frac{\mathbf{b}_{ik} \cdot \mathbf{e}_z}{\sin \theta} \equiv \frac{b_{ikz}}{\sin \theta}. \quad (65)$$

Consequently, Eq. (59) takes the following form:

$$\hat{\Omega}_{100}^{(i)} = h_i \sum_k \frac{b_{ikz}}{\sin \theta} L^{(k)}. \quad (66)$$

And the quantity $\hat{\Omega}_{001}^{(i)}$ is calculated according to Eq. (53):

$$\hat{\Omega}_{001}^{(i)} = h_i \hat{\Omega}_{000}^{(i)} \equiv h_i \Omega^{(i)}. \quad (67)$$

Finally, collecting Eqs. (64), (66), (67), one can get the following answer:

$$\Omega_{001}^{(i)} = h_i \sum_k b_{ikz} L^{(k)} + h_i n_{iz} \Omega^{(i)}. \quad (68)$$

This is an analytical representation of $\Omega_{001}^{(i)}$ in a closed form, because, as mentioned in Section IV, the primitives $L^{(k)}$ and $\Omega^{(i)}$ can be expressed through elementary functions.

VI. EVALUATION OF LINE INTEGRALS $L_{mnp}^{(k)}$

Let A_k and B_k be two end points of k th edge (we denote their radius vectors as $\mathbf{r}_A^{(k)}$ and $\mathbf{r}_B^{(k)}$), and \mathbf{l}_k be the unit vector directed from A_k to B_k . To find analytical expressions for the line integrals $L_{mnp}^{(k)}$, it is convenient to reduce them to more simple integrals $\mathcal{L}_t^{(k)}$:

$$\mathcal{L}_t^{(k)} = \int_{\xi_{k1}}^{\xi_{k2}} \frac{\xi^t}{\sqrt{\rho_k^2 + \xi^2}} d\xi, \quad (69)$$

where t is a non-negative integer number, $\xi = \mathbf{l}_k \cdot (\mathbf{r} - \mathbf{R})$ is a coordinate along k th edge, ρ_k is the distance from the point \mathbf{R} to the line of k th edge:

$$\rho_k^2 = |\mathbf{r}_A^{(k)} - \mathbf{R}|^2 - [\mathbf{l}_k \cdot (\mathbf{r}_A^{(k)} - \mathbf{R})]^2, \quad (70)$$

ξ_{k1} and ξ_{k2} are the values of ξ at A_k and B_k :

$$\xi_{k1} = \mathbf{l}_k \cdot (\mathbf{r}_A^{(k)} - \mathbf{R}), \quad \xi_{k2} = \mathbf{l}_k \cdot (\mathbf{r}_B^{(k)} - \mathbf{R}). \quad (71)$$

In order to perform such reduction, let us express the position vector \mathbf{r} of a point *on the edge* through the coordinate ξ :

$$\mathbf{r}(\xi) = \mathbf{r}_0^{(k)} + \mathbf{l}_k \xi, \quad (72)$$

where the point $\mathbf{r}_0^{(k)} = (x_0^{(k)}, y_0^{(k)}, z_0^{(k)})$ is the projection of the point \mathbf{R} to k th edge:

$$\mathbf{r}_0^{(k)} = \mathbf{r}_A^{(k)} - \mathbf{l}_k [\mathbf{l}_k \cdot (\mathbf{r}_A^{(k)} - \mathbf{R})]. \quad (73)$$

Using Eq. (72), one can represent the factor $(x-X)^m (y-Y)^n (z-Z)^p$ that appears in the definition of $L_{mnp}^{(k)}$ as follows:

$$(x-X)^m (y-Y)^n (z-Z)^p = (x_0^{(k)} - X + l_{k,x} \xi)^m (y_0^{(k)} - Y + l_{k,y} \xi)^n (z_0^{(k)} - Z + l_{k,z} \xi)^p. \quad (74)$$

The right hand side of Eq. (74) is some polynomial on ξ :

$$(x_0^{(k)} - X + l_{k,x} \xi)^m (y_0^{(k)} - Y + l_{k,y} \xi)^n (z_0^{(k)} - Z + l_{k,z} \xi)^p = \sum_{t=0}^{m+n+p} c_{mnp,t}(\mathbf{R}) \xi^t, \quad (75)$$

where each coefficient $c_{mnp,t}(\mathbf{R})$ is a polynomial of X, Y, Z of degree $m+n+p-t$. Substituting this series decomposition into the line integral $L_{mnp}^{(k)}$, Eq. (29), and taking into account that $|\mathbf{r} - \mathbf{R}| = \sqrt{\rho_k^2 + \xi^2}$ on the edge, one can easily see that

$$L_{mnp}^{(k)} = \sum_{t=0}^{m+n+p} c_{mnp,t}(\mathbf{R}) \mathcal{L}_t^{(k)}. \quad (76)$$

A similar representation takes place for the ‘‘tilted’’ line integrals $\hat{L}_{mnp}^{(k)}$ defined by Eq. (49c):

$$\hat{L}_{mnp}^{(k)} = \sum_{t=0}^{m+n+p} \hat{c}_{mnp,t}(\mathbf{R}) \mathcal{L}_t^{(k)}. \quad (77)$$

The coefficients $\hat{c}_{mnp,t}(\mathbf{R})$ are to be obtained from the identity

$$\begin{aligned} (\hat{x}_0^{(k)} + \hat{l}_{k,x} \xi)^m (\hat{y}_0^{(k)} + \hat{l}_{k,y} \xi)^n (\hat{z}_0^{(k)} + \hat{l}_{k,z} \xi)^p \\ = \sum_{t=0}^{m+n+p} \hat{c}_{mnp,t}(\mathbf{R}) \xi^t, \end{aligned} \quad (78)$$

where

$$\hat{x}_0^{(k)} = (\mathbf{r}_0^{(k)} - \mathbf{R}) \cdot \hat{\mathbf{e}}_x, \quad \hat{l}_{k,x} = \mathbf{l}_k \cdot \hat{\mathbf{e}}_x, \quad (79)$$

and the same for y - and z -components.

The last question is how to find analytical expressions for the integrals $\mathcal{L}_0^{(k)}, \mathcal{L}_1^{(k)}, \dots$. As explained in Appendix G, integration of Eq. (69) by parts provides the following recursive formula for $t > 1$:

$$\begin{aligned} \mathcal{L}_t^{(k)} = -\frac{t-1}{t} \rho_k^2 \mathcal{L}_{t-2}^{(k)} \\ + \frac{1}{t} [\mathbf{l}_k \cdot (\mathbf{r}_B^{(k)} - \mathbf{R})]^{t-1} |\mathbf{r}_B^{(k)} - \mathbf{R}| \\ - \frac{1}{t} [\mathbf{l}_k \cdot (\mathbf{r}_A^{(k)} - \mathbf{R})]^{t-1} |\mathbf{r}_A^{(k)} - \mathbf{R}|, \end{aligned} \quad (80)$$

and a simple answer for $t = 1$:

$$\mathcal{L}_1^{(k)} = |\mathbf{r}_B^{(k)} - \mathbf{R}| - |\mathbf{r}_A^{(k)} - \mathbf{R}|. \quad (81)$$

Eqs. (80) and (81) provide a possibility to evaluate the quantities $\mathcal{L}_t^{(k)}$ for integer $t \geq 0$ in terms of $\mathcal{L}_0^{(k)}$ and coordinates of the ends A_k and B_k of the edge. In its turn, $\mathcal{L}_0^{(k)}$ is the same as $L^{(k)}$ and therefore has the analytical representation according to Eq. (43). So, the problem of evaluating of line integrals along inclusion edges is solved.

VII. THE MAIN RESULT

Here we summarize the results of Sections II–V and present the analytical expression for the strain distribution that solves the problem posed in the Introduction.

At first, let us recall the steps carried out in the above text. In Section II, the strain tensor $\varepsilon_{\alpha\beta}(\mathbf{R})$ was expressed in terms of second derivatives of the electrostatic potential $\varphi(\mathbf{R})$. In Section III, these second derivatives, as well as the first derivatives and the potential itself, were represented as combinations of the quantities φ_{mnp} , $\varphi_{,\alpha}^{(mnp)}$, $\varphi_{,\alpha\beta}^{(mnp)}$, which correspond to the charge distribution $(x - X)^m(y - Y)^n(z - Z)^p \chi(\mathbf{r})$. These quantities, in their turn, were reduced in Section IV to four kinds of “primitives”: volume integrals φ_{mnp} , surface integrals $\Phi_{mnp}^{(i)}$ and $\Omega_{mnp}^{(k)}$, and line integrals $L_{mnp}^{(k)}$. In Section V, the volume and surface integrals were expressed through the solid angles $\Omega^{(i)}$ and line integrals $\hat{L}_{mnp}^{(k)}$. Finally, in Section VI all the line integrals $L_{mnp}^{(k)}$ and $\hat{L}_{mnp}^{(k)}$ were reduced to the simplest line integrals $L^{(k)}$, whose analytical representations are given by Eq. (43), and to the distances from the point \mathbf{R} (where the strain tensor is to be found) to vertices of the polyhedron.

Each of these steps represents itself a linear transformation whose coefficients are either constants (such as components of unit vectors \mathbf{n}_i in Eq. (30)) or polynomials of \mathbf{R} (for example, the factor $h_i = (\mathbf{r}_i - \mathbf{R}) \cdot \mathbf{n}_i$ in Eq. (47)).

As a result, the strain tensor $\varepsilon_{\alpha\beta}(\mathbf{R})$ appears to be a linear combination of three kinds of analytical functions:

- surface integrals (potentials of the inclusion faces covered by uniform double layers) $\Omega^{(i)}(\mathbf{R}) \equiv \Omega_{000}^{(i)}(\mathbf{R})$ defined according to Eq. (28) and having a geometrical meaning of solid angles;
- line integrals (potentials of uniformly charged edges of the inclusion) $L^{(k)}(\mathbf{R}) \equiv L_{000}^{(k)}(\mathbf{R})$ that have the analytical form according to Eq. (43);
- distances $|\mathbf{R} - \mathbf{r}_s|$ between the point \mathbf{R} and vertices \mathbf{r}_s of the inclusion (we will use the index s to number the vertices).

The same is true for the potential $\varphi(\mathbf{R})$ and its first and second derivatives on \mathbf{R} . The coefficients at quantities $\Omega^{(i)}$, $L^{(k)}$ and $|\mathbf{R} - \mathbf{r}_s|$ come from substituting polynomial expressions one into the other, and therefore should be polynomials of \mathbf{R} .

The facts described in this Section constitute the main result of the present study. In Subsection VII A we represent them in a more formal way, writing down the analytical expressions that define the distributions of the strain, the potential, and derivatives of the potential, up to some polynomial coefficients. Then, in Subsection VII B we will show how to find these polynomial coefficients.

A. The main result: Analytical expressions for the strain distribution, the potential, and its derivatives

Based on the above-presented considerations, one can formulate a universal expression for the strain distribution $\varepsilon_{\alpha\beta}(\mathbf{R})$ induced by a polyhedral inclusion with a

lattice misfit $\varepsilon_0(\mathbf{R})$ that depends on coordinates polynomially:

$$\varepsilon_{\alpha\beta}(\mathbf{R}) = \sum_{\substack{i \\ (\text{faces})}} \mathcal{A}_{\varepsilon_{\alpha\beta}}^{(i)} \Omega^{(i)} + \sum_{\substack{k \\ (\text{edges})}} \mathcal{B}_{\varepsilon_{\alpha\beta}}^{(k)} L^{(k)} + \sum_{\substack{s \\ (\text{vertices})}} \mathcal{C}_{\varepsilon_{\alpha\beta}}^{(s)} |\mathbf{R} - \mathbf{r}_s|. \quad (82)$$

Here summations take place over all faces (index i), edges (index k), and vertices (index s) of the polyhedron. $\Omega^{(i)}(\mathbf{R})$ and $L^{(k)}(\mathbf{R})$ are analytical functions described in Section IV: $\Omega^{(i)}$ has a geometrical meaning of a solid angle, and $L^{(k)}$ is defined by Eq. (43). \mathbf{r}_s is a position vector of s th vertex. $\mathcal{A}_{\varepsilon_{\alpha\beta}}^{(i)}(\mathbf{R})$, $\mathcal{B}_{\varepsilon_{\alpha\beta}}^{(k)}(\mathbf{R})$, $\mathcal{C}_{\varepsilon_{\alpha\beta}}^{(s)}(\mathbf{R})$ are some polynomial functions of \mathbf{R} that are defined by orientations of faces and edges and by coordinates of vertices. The degrees of polynomials $\mathcal{A}_{\varepsilon_{\alpha\beta}}^{(i)}$ and $\mathcal{B}_{\varepsilon_{\alpha\beta}}^{(k)}$ are equal to N , i. e., to the degree of the polynomial $f(\mathbf{r})$ that determines the distribution of lattice misfit, whereas degrees of $\mathcal{C}_{\varepsilon_{\alpha\beta}}^{(s)}$ are equal to $N - 1$. (if $N = 0$, that corresponds to a constant lattice misfit, then $\mathcal{C}_{\varepsilon_{\alpha\beta}}^{(s)} = 0$ at any \mathbf{R} .) A recipe for calculation of the polynomial coefficients of $\mathcal{A}_{\varepsilon_{\alpha\beta}}^{(i)}$, $\mathcal{B}_{\varepsilon_{\alpha\beta}}^{(k)}$ and $\mathcal{C}_{\varepsilon_{\alpha\beta}}^{(s)}$ will be described in Subsection VII B. Of course, Eq. (82) is valid only if the assumptions listed in the Introduction are fulfilled.

In a fully analogous manner, one can write down a similar expression for the electrostatic potential φ [a solution of Poisson’s equation (7)] produced by a charged polyhedron with a non-uniform charge distribution $\varepsilon(\mathbf{R})$, which is a polynomial function of coordinates:

$$\varphi(\mathbf{R}) = \sum_{\substack{i \\ (\text{faces})}} \mathcal{A}_{\varphi}^{(i)} \Omega^{(i)} + \sum_{\substack{k \\ (\text{edges})}} \mathcal{B}_{\varphi}^{(k)} L^{(k)} + \sum_{\substack{s \\ (\text{vertices})}} \mathcal{C}_{\varphi}^{(s)} |\mathbf{R} - \mathbf{r}_s|, \quad (83)$$

where polynomials $\mathcal{A}_{\varphi}^{(i)}(\mathbf{R})$ and $\mathcal{B}_{\varphi}^{(k)}(\mathbf{R})$ have the degree $N + 2$, and polynomials $\mathcal{C}_{\varphi}^{(s)}(\mathbf{R})$ have the degree $N + 1$.

The first and second derivatives of the potential $\varphi(\mathbf{R})$ also have similar representations:

$$\frac{\partial \varphi(\mathbf{R})}{\partial R_{\alpha}} = \sum_{\substack{i \\ (\text{faces})}} \mathcal{A}_{\varphi_{\alpha}}^{(i)} \Omega^{(i)} + \sum_{\substack{k \\ (\text{edges})}} \mathcal{B}_{\varphi_{\alpha}}^{(k)} L^{(k)} + \sum_{\substack{s \\ (\text{vertices})}} \mathcal{C}_{\varphi_{\alpha}}^{(s)} |\mathbf{R} - \mathbf{r}_s| \quad (84)$$

and

$$\frac{\partial^2 \varphi(\mathbf{R})}{\partial R_{\alpha} \partial R_{\beta}} = \sum_{\substack{i \\ (\text{faces})}} \mathcal{A}_{\varphi_{\alpha\beta}}^{(i)} \Omega^{(i)} + \sum_{\substack{k \\ (\text{edges})}} \mathcal{B}_{\varphi_{\alpha\beta}}^{(k)} L^{(k)} + \sum_{\substack{s \\ (\text{vertices})}} \mathcal{C}_{\varphi_{\alpha\beta}}^{(s)} |\mathbf{R} - \mathbf{r}_s|, \quad (85)$$

where $\mathcal{A}_{\varphi\alpha}^{(i)}(\mathbf{R})$ and $\mathcal{B}_{\varphi\alpha}^{(k)}(\mathbf{R})$ are polynomials of degree $N + 1$; $\mathcal{C}_{\varphi\alpha}^{(s)}(\mathbf{R})$, $\mathcal{A}_{\varphi\alpha\beta}^{(i)}(\mathbf{R})$ and $\mathcal{B}_{\varphi\alpha\beta}^{(k)}(\mathbf{R})$ are polynomials of degree N ; and $\mathcal{C}_{\varphi\alpha\beta}^{(s)}(\mathbf{R})$ are polynomials of degree $N - 1$. The coefficients of all these polynomials are to be calculated by the method of Subsection VII B.

B. The main result: Algorithm of finding the polynomial coefficients

Equations (82)–(85) determine the sought-for functions $\varepsilon_{\alpha\beta}(\mathbf{R})$, $\varphi(\mathbf{R})$, $\partial\varphi(\mathbf{R})/\partial R_\alpha$ and $\partial^2\varphi(\mathbf{R})/\partial R_\alpha\partial R_\beta$ up to the coefficients of the corresponding polynomials \mathcal{A} , \mathcal{B} , \mathcal{C} . Here we represent the algorithm (a sequence of steps) for calculating these coefficients. The algorithm is just a summary of equations obtained in previous sections.

On the input of the algorithm there are: the polynomial function $f(x, y, z)$, which defines the distribution of eigenstrain inside the inclusion, and the geometry of the inclusion—unit vectors \mathbf{n}_i , \mathbf{b}_{ik} , \mathbf{l}_k and coordinates of vertices.

On the output there are polynomials $\mathcal{A}_{\varepsilon\alpha\beta}^{(i)}(\mathbf{R})$, $\mathcal{B}_{\varepsilon\alpha\beta}^{(k)}(\mathbf{R})$, $\mathcal{C}_{\varepsilon\alpha\beta}^{(s)}(\mathbf{R})$ that determine the distribution of elastic strain $\varepsilon_{\alpha\beta}(\mathbf{R})$ according to Eq. (82). For finding the polynomials related to the potential and its derivatives, one should modify Steps 1–3, as explained in the end of this Subsection.

The algorithm consists of eleven steps listed below. Each step contains only arithmetic operations on polynomials. Therefore, it is easy to implement the algorithm in a program code.

Step 1. Express strain components $\varepsilon_{\alpha\beta}$ via second derivatives $\partial^2\varphi/\partial R_\alpha\partial R_\beta$ using Eq. (12); express the function ε_0 that appears in the right-hand side of Eq. (12) via solid angles $\Omega^{(i)}$ using Eq. (42).

Step 2. Find the coefficients $\tilde{C}_{mnp}(\mathbf{R})$ from Eq. (19), and represent the second derivatives $\partial^2\varphi/\partial R_\alpha\partial R_\beta$ as combinations of $\varphi_{,\alpha\beta}^{(mnp)}$ using Eq. (22).

Step 3. Express each of the quantities $\varphi_{,\alpha\beta}^{(mnp)}$ through integrals $\varphi_{m'n'p'}$, $\Phi_{m'n'p'}^{(i)}$, $\Omega_{m'n'p'}^{(i)}$ and $L_{m'n'p'}^{(k)}$ with different m', n', p' according to Eqs. (34), (37), (38).

Step 4. Reduce each of the volume integrals φ_{mnp} to a combination of surface integrals $\Phi_{mnp}^{(i)}$ using Eq. (47). (After this step the strain tensor, as a function of coordinates, is represented as a linear combination of functions $\Phi_{mnp}^{(i)}$, $\Omega_{mnp}^{(i)}$, $L_{mnp}^{(k)}$ with polynomial coefficients.)

Steps 5–9 should be performed for each face i of the inclusion:

Step 5. Choose a “tilted” coordinate system $\hat{x}, \hat{y}, \hat{z}$ with axis \hat{z} along the normal \mathbf{n}_i to i th face. Then, transform the integrals $\Phi_{mnp}^{(i)}$ and $\Omega_{mnp}^{(i)}$ into their “tilted” versions $\hat{\Phi}_{mnp}^{(i)}$ and $\hat{\Omega}_{mnp}^{(i)}$ using Eqs. (50a) and (50b). The coefficients of transformation $T_{mnp}^{m'n'p'}$ are to be found from the identity (51).

Step 6. Decrease the index p at $\hat{\Phi}_{mnp}^{(i)}$ and $\hat{\Omega}_{mnp}^{(i)}$ down to zero by means of Eq. (53).

Step 7. Express the integrals $\hat{\Phi}_{mn0}^{(i)}$ via $\hat{\Omega}_{mn0}^{(i)}$ and $\hat{L}_{mn0}^{(k)}$ using Eq. (55). (After this step, the strain distribution is expressed in terms of surface integrals $\hat{\Omega}_{mn0}^{(i)}$ and line integrals $L_{mnp}^{(k)}$, $\hat{L}_{mn0}^{(k)}$.)

Step 8. For each $\hat{\Omega}_{mn0}^{(i)}$, decrease the index n recursively down to $n = 1$ or $n = 0$ by means of Eq. (56). Then, if $n = 1$, express the quantity $\hat{\Omega}_{m10}^{(i)}$ via $\hat{L}_{m00}^{(k)}$ using Eq. (57).

Step 9. For each $\hat{\Omega}_{m00}^{(i)}$, decrease the index m recursively down to $m = 1$ or $m = 0$ by means of Eq. (58). Then, if $m = 1$, express the quantity $\hat{\Omega}_{100}^{(i)}$ via $L^{(k)}$ using Eq. (59). (After this step, the strain distribution appears to be a combination of solid angles $\Omega^{(i)}$ and line integrals $L_{mnp}^{(k)}$, $\hat{L}_{mn0}^{(k)}$.)

Step 10. For each edge k of the inclusion, decompose each line integral $L_{mnp}^{(k)}$ into a series $c_{mnp,0}\mathcal{L}_0^{(k)} + c_{mnp,1}\mathcal{L}_1^{(k)} + \dots$ according to Eq. (76), where coefficients $c_{mnp,0}(\mathbf{R})$, $c_{mnp,1}(\mathbf{R})$, \dots are to be found from Eq. (75). Do the same with “tilted” line integrals $\hat{L}_{mn0}^{(k)}$ by means of Eqs. (77), (78).

Step 11. For each edge k and each line integral $\mathcal{L}_t^{(k)}$, decrease the index t recursively down to $t = 1$ or $t = 0$ by means of Eq. (80). Then, if $t = 1$, evaluate the integral $\mathcal{L}_1^{(k)}$ using Eq. (81).

After performing Steps 1–11, one obtains the strain distribution $\varepsilon_{\alpha\beta}(\mathbf{R})$ in the form of a combination of solid angles $\Omega^{(i)}(\mathbf{R})$, logarithmic expressions $L^{(k)}(\mathbf{R})$, and distances from \mathbf{R} to inclusion vertices, i. e., in the form of Eq. (82) with the *known* polynomial coefficients $\mathcal{A}_{\varepsilon\alpha\beta}^{(i)}(\mathbf{R})$, $\mathcal{B}_{\varepsilon\alpha\beta}^{(k)}(\mathbf{R})$, $\mathcal{C}_{\varepsilon\alpha\beta}^{(s)}(\mathbf{R})$. Hence, these steps actually constitute an algorithm for calculating the polynomials \mathcal{A} , \mathcal{B} , \mathcal{C} .

In Appendix J, one can find an example of implementation of this algorithm in the form of an informal “pseudocode”.

In a slightly modified form, this algorithm can be also used to calculate the potential $\varphi(\mathbf{R})$, its derivatives and its second derivatives. For that, it is enough to omit Step 1 and make obvious modifications of Steps 2 and 3. Namely, for finding an expression for the potential $\varphi(\mathbf{R})$, one can use Eq. (20) instead of Eq. (22), and omit Step 3. For finding the expressions for the first derivatives $\partial\varphi(\mathbf{R})/\partial R_\alpha$, one can use Eq. (21) instead of Eq. (22) at Step 2, and Eqs. (30), (32) instead of Eqs. (34), (37), (38) at Step 3.

VIII. EXAMPLES

This Section has two aims: (i) to illustrate the results of Section VII on concrete examples, and (ii) to provide the evidence that our results are correct.

A. Constant lattice misfit

For the simplest example, let us suppose that the lattice parameter is the same in any point of the inclusion. Therefore

$$f = \text{const}, \quad (86)$$

and the lattice misfit ε_0 is equal to f inside the inclusion, and to 0 outside. Applying the algorithm of Section VII to this case, one can see that the answer for the strain distribution in the form (82) appears already after Step 3:

$$\begin{aligned} \varepsilon_{\alpha\beta}(\mathbf{R}) = & -\Lambda f \sum_i n_{i\alpha} n_{i\beta} \Omega^{(i)}(\mathbf{R}) \\ & -\Lambda f \sum_k \lambda_{\alpha\beta}^{(k)} L^{(k)}(\mathbf{R}) + \frac{f}{4\pi} \delta_{\alpha\beta} \sum_i \Omega^{(i)}(\mathbf{R}), \end{aligned} \quad (87)$$

where values of Λ and $\lambda_{\alpha\beta}^{(k)}$ are defined by Eqs. (10) and (33). A similar result was reported in Ref. 37.

A comparison between Eq. (82) and Eq. (87) provides the values of the coefficients \mathcal{A} , \mathcal{B} , \mathcal{C} for the case of a constant lattice misfit inside the inclusion:

$$\mathcal{A}_{\varepsilon_{\alpha\beta}}^{(i)} = -\Lambda f n_{i\alpha} n_{i\beta} + \delta_{\alpha\beta} f / 4\pi, \quad (88a)$$

$$\mathcal{B}_{\varepsilon_{\alpha\beta}}^{(k)} = -\Lambda f \lambda_{\alpha\beta}^{(k)}, \quad (88b)$$

$$\mathcal{C}_{\varepsilon_{\alpha\beta}}^{(s)} = 0. \quad (88c)$$

For better understanding of the way leading to this answer, one can visualize the algorithm in the form of a tree, as shown in the left part of Fig. 6. The sought-for function $\varepsilon_{\alpha\beta}$ is placed at the top of this graph. At Step 1, this function acquires the following representation:

$$\varepsilon_{\alpha\beta} = -\Lambda \frac{\partial^2 \varphi}{\partial R_\alpha \partial R_\beta} + \sum_i \frac{\delta_{\alpha\beta} f}{4\pi} \Omega^{(i)}, \quad (89)$$

that is symbolized in the graph by arrows connecting $\varepsilon_{\alpha\beta}$ to $\partial^2 \varphi / \partial R_\alpha \partial R_\beta$ and to $\Omega^{(i)}$. A value near an arrow means the factor, with which the expression on the head of the arrow contributes to the expression on the tail. Then, Step 2 represents $\partial^2 \varphi / \partial R_\alpha \partial R_\beta$ as follows:

$$\frac{\partial^2 \varphi}{\partial R_\alpha \partial R_\beta} = f \varphi_{,\alpha\beta}^{(000)}. \quad (90)$$

This connection is shown in the graph by the arrow with mark “ f ”. Finally, Step 3 provides the expression for $\varphi_{,\alpha\beta}^{(000)}$:

$$\varphi_{,\alpha\beta}^{(000)} = \sum_i n_{i\alpha} n_{i\beta} \Omega^{(i)} + \sum_l \lambda_{\alpha\beta}^{(k)} L^{(k)}, \quad (91)$$

which is depicted by two lower arrows in the graph.

The formulas for the coefficients \mathcal{A} , \mathcal{B} , \mathcal{C} can be easily constructed on the basis of this graph. Each appearance of $\Omega^{(i)}$ or $L^{(k)}$ in the graph provides the contribution to

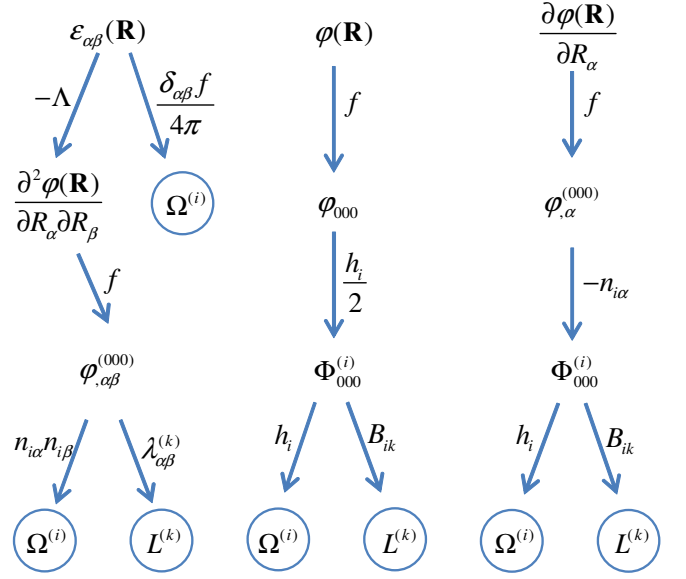


FIG. 6. Schematic representation of the algorithm of calculating the strain tensor $\varepsilon_{\alpha\beta}$ (left part), the potential φ (middle part), derivatives of the potential $\partial\varphi/\partial R_\alpha$ (right part), and second derivatives of the potential $\partial^2\varphi/\partial R_\alpha\partial R_\beta$ (a sub-graph of the left part) in the case of a uniform eigenstrain: $f = \text{const}$. See details in Subsection VIII A.

$\mathcal{A}_{\varepsilon_{\alpha\beta}}^{(i)}$ or $\mathcal{B}_{\varepsilon_{\alpha\beta}}^{(k)}$, correspondingly. The value of the contribution is equal to the product of the quantities on arrows along the way from the root of the tree to $\Omega^{(i)}$ or $L^{(k)}$. For example, the way to $L^{(k)}$ consists of three arrows with values $-\Lambda$, f and $\lambda_{\alpha\beta}^{(k)}$ on them; hence, their product $-\Lambda f \lambda_{\alpha\beta}^{(k)}$ appears in Eq. (88b).

In a similar manner, one can calculate the potential of a uniformly charged polyhedral body $\varphi(\mathbf{R})$, and its first and second derivatives. Since f is a constant ($N = 0$), only primitives with $m = n = p = 0$ will appear in the course of the algorithm. For this reason, one can omit Steps 5, 6, 8–11 (as well as Step 1, which is needed only for calculating the strain). The result for the potential is

$$\mathcal{A}_\varphi^{(i)}(\mathbf{R}) = \frac{f}{2} (h_i)^2, \quad (92a)$$

$$\mathcal{B}_\varphi^{(k)}(\mathbf{R}) = \frac{f}{2} (h_{i_1} B_{i_1 k} + h_{i_2} B_{i_2 k}), \quad (92b)$$

$$\mathcal{C}_\varphi^{(s)}(\mathbf{R}) = 0, \quad (92c)$$

where i_1 and i_2 are numbers of the two faces that intersect at k th edge; the linear functions $h_i(\mathbf{R})$ and $B_{ik}(\mathbf{R})$ are defined by Eqs. (44) and (45), correspondingly. Expressions (92) are to be inserted into the general formula (83).

For the first derivatives of the potential, the answer is:

$$\mathcal{A}_{\varphi\alpha}^{(i)}(\mathbf{R}) = -fn_{i\alpha}h_i, \quad (93a)$$

$$\mathcal{B}_{\varphi\alpha}^{(k)}(\mathbf{R}) = -f(n_{i_1\alpha}B_{i_1k} + n_{i_2\alpha}B_{i_2k}), \quad (93b)$$

$$\mathcal{C}_{\varphi\alpha}^{(s)}(\mathbf{R}) = 0, \quad (93c)$$

and there is the answer for the second derivatives of the potential:

$$\mathcal{A}_{\varphi\alpha\beta}^{(i)} = fn_{i\alpha}n_{i\beta}, \quad (94a)$$

$$\mathcal{B}_{\varphi\alpha\beta}^{(k)} = f\lambda_{\alpha\beta}^{(k)}, \quad (94b)$$

$$\mathcal{C}_{\varphi\alpha\beta}^{(s)} = 0. \quad (94c)$$

In Fig. 6 one can see also graphical representations for the potential φ (middle part), its derivative $\partial\varphi/\partial R_\alpha$ (right part), and its second derivative $\partial^2\varphi/\partial R_\alpha\partial R_\beta$ (the part of the left graph, beginning from $\partial^2\varphi/\partial R_\alpha\partial R_\beta$).

Our expressions (92)–(94) for the potential of a homogeneous polyhedron and its first and second derivatives are the same as the results by Werner and Scheeres.⁵¹ One can consider the coincidence of our results for $f = \text{const}$ with the published ones as a simplest test on the correctness of our approach. According to the present Subsection, this test is successfully passed.

Also we have performed a comparison with analytical calculations made by Glas¹² for the case of a truncated pyramid with a constant misfit strain. The results of calculations shown in Fig. 3b of Ref. 12 are fully reproduced by our method. For more details, see Appendix H.

B. Constant, vertically directed gradient of the lattice misfit

Now let us examine the case of linear dependence of the eigenstrain ε_0 on the coordinates inside the inclusion. For simplicity, we suppose in this Subsection that the eigenstrain depends on coordinate z only:

$$f(x, y, z) = az + b, \quad (95)$$

where a (the gradient of the eigenstrain) and b are constants. For such a function $f(\mathbf{r})$, the algorithm of Section VII is shown in a graphical form in Fig. 7. The meaning of arrows and expressions in the nodes of the graph is explained above, see the caption to Fig. 6. In the part of the tree below $\Omega_{001}^{(i)}$, we use the results of Subsection V A. For the arrow connecting $\mathcal{L}_1^{(k)}$ to $|\mathbf{R} - \mathbf{r}_s|$, the factor is equal to $+1$ if the vector \mathbf{l}_k is directed from the opposite vertex of k th edge to s th vertex, and -1 otherwise.

The expressions for the polynomials $\mathcal{A}_{\varepsilon\alpha\beta}^{(i)}$, $\mathcal{B}_{\varepsilon\alpha\beta}^{(k)}$, $\mathcal{C}_{\varepsilon\alpha\beta}^{(s)}$ can be derived from the graph in Fig. 7 by the method described in Subsection VIII A. The only new feature is the existence of a node $|\mathbf{R} - \mathbf{r}_s|$ that provides a contribution to the polynomial $\mathcal{C}_{\varepsilon\alpha\beta}^{(s)}$, which is equal to the product of

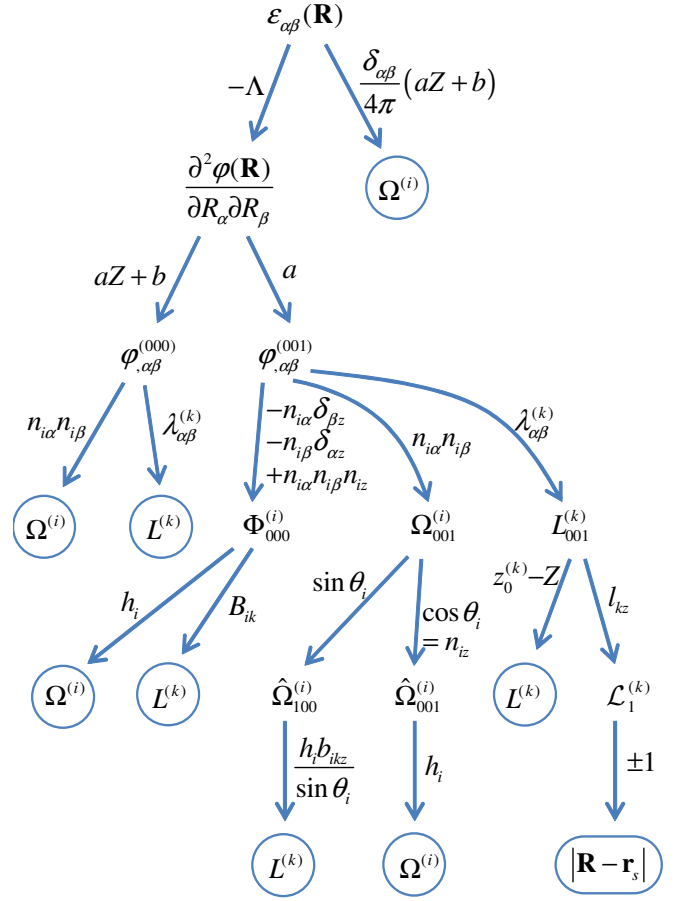


FIG. 7. Schematic representation of the algorithm of calculating the strain tensor $\varepsilon_{\alpha\beta}$ in the case of a linearly varied eigenstrain: $f = az + b$.

the quantities near the arrows on the way from $\varepsilon_{\alpha\beta}$ to $|\mathbf{R} - \mathbf{r}_s|$. As a result, one can get the following answers for $\mathcal{A}_{\varepsilon\alpha\beta}^{(i)}$, $\mathcal{B}_{\varepsilon\alpha\beta}^{(k)}$ and $\mathcal{C}_{\varepsilon\alpha\beta}^{(s)}$:

$$\begin{aligned} \mathcal{A}_{\varepsilon\alpha\beta}^{(i)}(\mathbf{R}) &= -\Lambda(aZ + b)n_{i\alpha}n_{i\beta} \\ &- \Lambda a (-n_{i\alpha}\delta_{\beta z} - n_{i\beta}\delta_{\alpha z} + 2n_{i\alpha}n_{i\beta}n_{iz})h_i + (aZ + b)\frac{\delta_{\alpha\beta}}{4\pi}, \end{aligned} \quad (96a)$$

$$\begin{aligned} \mathcal{B}_{\varepsilon\alpha\beta}^{(k)}(\mathbf{R}) &= -\Lambda(aZ + b)\lambda_{\alpha\beta}^{(k)} \\ &- \Lambda a \sum_i (-n_{i\alpha}\delta_{\beta z} - n_{i\beta}\delta_{\alpha z} + n_{i\alpha}n_{i\beta}n_{iz})B_{ik} \\ &- \Lambda a \sum_i n_{i\alpha}n_{i\beta}b_{ikz}h_i - \Lambda a \lambda_{\alpha\beta}^{(k)}(z_0^{(k)} - Z), \end{aligned} \quad (96b)$$

where index i runs over the two faces adjacent to k th edge,

$$\mathcal{C}_{\varepsilon\alpha\beta}^{(s)}(\mathbf{R}) = -\Lambda a \sum_k \lambda_{\alpha\beta}^{(k)}(\pm l_{kz}), \quad (96c)$$

where index k runs over the edges that enter s th vertex. The sign in the factor $(\pm l_{kz})$ is chosen to be plus if the vector \mathbf{l}_k is directed from the opposite vertex of k th edge to s th vertex, and minus otherwise. Constants Λ , $\lambda_{\alpha\beta}^{(k)}$, and linear functions $h_i(\mathbf{R})$, $B_{ik}(\mathbf{R})$, $z_0^{(k)}(\mathbf{R})$ are defined by Eqs. (10), (33), (44), (45), (73), correspondingly.

In the next Subsection, these equations will be generalized to the case of an arbitrarily directed gradient of the lattice misfit.

C. Constant gradient of the lattice misfit: general case

Consider the general case of a constant gradient of the lattice misfit inside the polyhedral inclusion:

$$f(\mathbf{r}) = \mathbf{a} \cdot \mathbf{r} + b, \quad (97)$$

where a vector \mathbf{a} and a scalar b are constants. It is easy to generalize formulas (96a)–(96c) to this case. For this purpose, it is enough to represent them in a coordinate-independent form, i. e., to replace the product aZ by $\mathbf{a} \cdot \mathbf{R}$, the product an_{iz} by $\mathbf{a} \cdot \mathbf{n}_i$, etc. This gives rise to the following result:

$$\begin{aligned} \mathcal{A}_{\varepsilon\alpha\beta}^{(i)}(\mathbf{R}) &= -\Lambda n_{i\alpha} n_{i\beta} [\mathbf{a} \cdot \mathbf{R} + b + 2(\mathbf{a} \cdot \mathbf{n}_i) h_i] \\ &+ \Lambda (a_\alpha n_{i\beta} + a_\beta n_{i\alpha}) h_i + (\mathbf{a} \cdot \mathbf{R} + b) \frac{\delta_{\alpha\beta}}{4\pi}, \end{aligned} \quad (98a)$$

$$\begin{aligned} \mathcal{B}_{\varepsilon\alpha\beta}^{(k)}(\mathbf{R}) &= -\Lambda \lambda_{\alpha\beta}^{(k)} (\mathbf{a} \cdot \mathbf{r}_0^{(k)} + b) \\ &+ \Lambda \sum_i (a_\alpha n_{i\beta} + a_\beta n_{i\alpha}) B_{ik} \\ &- \Lambda \sum_i n_{i\alpha} n_{i\beta} [(\mathbf{a} \cdot \mathbf{n}_i) B_{ik} + (\mathbf{a} \cdot \mathbf{b}_{ik}) h_i], \end{aligned} \quad (98b)$$

$$\mathcal{C}_{\varepsilon\alpha\beta}^{(s)}(\mathbf{R}) = -\Lambda \sum_k \lambda_{\alpha\beta}^{(k)} (\pm \mathbf{a} \cdot \mathbf{l}_k). \quad (98c)$$

In order to get the strain distribution $\varepsilon_{\alpha\beta}(\mathbf{R})$, one should insert these expressions into the universal equation (82).

By the same method, one can get the analytical formulas for the potential φ (as well as its first and second derivatives) of a non-uniformly charged polyhedral body with a charge density $\mathbf{a} \cdot \mathbf{r} + b$. The polynomials $\mathcal{A}_\varphi^{(i)}$, $\mathcal{B}_\varphi^{(k)}$ and $\mathcal{C}_\varphi^{(s)}$ related to the potential are expressed as follows:

$$\mathcal{A}_\varphi^{(i)}(\mathbf{R}) = \left(\frac{\mathbf{a} \cdot \mathbf{R} + b}{2} + \frac{(\mathbf{a} \cdot \mathbf{n}_i) h_i}{3} \right) h_i^2, \quad (99a)$$

$$\begin{aligned} \mathcal{B}_\varphi^{(k)}(\mathbf{R}) &= \frac{1}{6} \sum_i \left[\mathbf{a} \cdot (2\mathbf{R} + \mathbf{n}_i h_i + \mathbf{r}_0^{(k)}) + 3b \right] h_i B_{ik} \\ &+ \frac{1}{6} \sum_i (\mathbf{a} \cdot \mathbf{b}_{ik}) h_i^3, \end{aligned} \quad (99b)$$

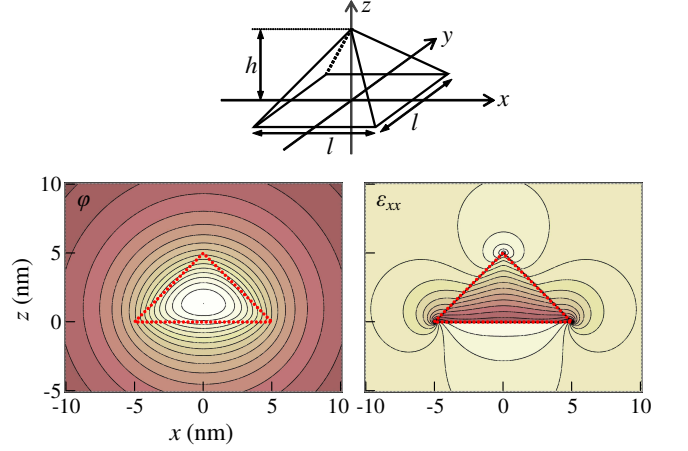


FIG. 8. Isoline plots (in the plane $y = 0$) of the potential $\varphi(\mathbf{r})$ and the strain component $\varepsilon_{xx}(\mathbf{r})$ produced by a pyramidal inclusion with height $h = 5$ nm and the length of the square base $l = 10$ nm. The eigenstrain $\varepsilon_0(\mathbf{r})$ inside the inclusion decreases linearly from the base to the apex: $\varepsilon_0 \propto (1 - z/2h)$. Poisson ratio $\nu = 0.25$. The potential is calculated via Eqs. (83), (99), and the strain—via Eqs. (82), (98). The isolines are equidistant in φ and ε_{xx} , brighter areas correspond to larger values. The inclusion cross section is shown by the red dotted contour.

$$\mathcal{C}_\varphi^{(s)}(\mathbf{R}) = \frac{1}{6} \sum_k \left[(\pm \mathbf{a} \cdot \mathbf{l}_k) \sum_i h_i B_{ik} \right]. \quad (99c)$$

Eqs. (99a)–(99c) are to be inserted into Eq. (83) in order to get the potential $\varphi(\mathbf{R})$.

Analytical expressions for the gravitational potential of a polyhedral body having a linearly varying density distribution were reported by many authors.^{43–47} However these expressions were not represented in terms of solid angles. For this reason, it seems to be extremely difficult to compare them directly with our answer [a combination of Eqs. (83) and (99)] at the level of formulas. To ensure that the results of this Subsection are correct, we performed numerical tests, considering a pyramid with a square base as an example of an inclusion (see Fig. 8). The following statements were checked numerically:

- $\varphi(x, y, z)$ is a continuous function, and its first derivatives are continuous;
- $\varphi(x, y, z)$ obeys Poisson's equation $\Delta\varphi = -4\pi\varepsilon_0$, where $\varepsilon_0(\mathbf{r}) = \mathbf{a} \cdot \mathbf{r} + b$ inside the pyramid, and $\varepsilon_0 = 0$ outside the pyramid;
- the functions $\varphi(x, y, z)$ and $\varepsilon_{\alpha\beta}(x, y, z)$ are connected to each other by Eq. (12).

The potential φ and the strain $\varepsilon_{\alpha\beta}$ were calculated by Eqs. (83), (99) and Eqs. (82), (98), correspondingly. The pyramid height h , the length l of the edge of the pyramid base, the gradient \mathbf{a} of the lattice misfit, and the free term b were varied independently. An example of the

calculated potential φ and xx -component of the strain is shown in Fig. 8 for the case of $h = 5$ nm, $l = 10$ nm, $a_x = a_y = 0$, and $a_z = -b/2h$. (Such a choice of \mathbf{a} means that the lattice misfit linearly decreases from the base to the apex of the pyramid, so that at the apex it is twice smaller than at the base.) For this case, as well as for many other combinations of parameters h , l , \mathbf{a} and b , the numerical test has been passed successfully.

In order to provide more evidences of validity of analytical results, we have compared the distribution of ε_{xx} calculated analytically and shown in Fig. 8 with analogous distributions calculated numerically using the finite element method. This comparison is presented in Appendix I. One can see that for large enough size of the “box”, in which the inclusion is incorporated, the numerical results perfectly agree with the analytical ones.

D. Sinusoidal profile of the lattice misfit

As an example of a more complicated distribution of the lattice misfit $\varepsilon_0(x, y, z)$, let us consider the sinusoidal profile inside the inclusion:

$$\varepsilon_0(\mathbf{r}) = \begin{cases} A \sin(kx) & \text{if } \mathbf{r} \text{ is inside the inclusion,} \\ 0 & \text{if } \mathbf{r} \text{ is outside the inclusion,} \end{cases} \quad (100)$$

so that $f(\mathbf{r}) = A \sin(kx)$, where A is a constant. In order to apply the results of the present paper, one has to approximate the function $f(\mathbf{r})$ by a polynomial. As such an approximation, we choose first five terms of the Fourier series,

$$f(\mathbf{r}) \approx A \left[kx - \frac{(kx)^3}{3!} + \frac{(kx)^5}{5!} - \frac{(kx)^7}{7!} + \frac{(kx)^9}{9!} \right], \quad (101)$$

that provides accuracy not worse than one percent of A within one period, i. e., for $|kx| \leq \pi$.

In Fig. 9, an example of the potential $\varphi(x, y, z)$, its derivatives $\partial\varphi/\partial x$ and $\partial^2\varphi/\partial x^2$, and the xx -component of the strain tensor is shown for the same pyramidal inclusion as in Fig. 8. The height h and the lateral size l of the pyramid are 5 nm and 10 nm, correspondingly. The parameter k is chosen to be $k = 2\pi/l$, so that the pyramid size l corresponds to the period of the sinusoid.

The values of the strain tensor, the potential, and its first and second derivatives were calculated by Eqs. (82)–(85). The coefficients of polynomials \mathcal{A} , \mathcal{B} , \mathcal{C} , which contribute to these equations, were calculated numerically, directly following the algorithm of Subsection VII B. Then, the same numerical test as for a linearly varying eigenstrain (see the previous Subsection) was performed and successfully passed. In addition, it was checked that the results for the potential and its first and second derivatives are consistent with each other.

Such a numerical test with a degree N of the polynomial $f(\mathbf{r})$, larger than 1, is important for the following reason. Equations (56), (58) and (80) are used at

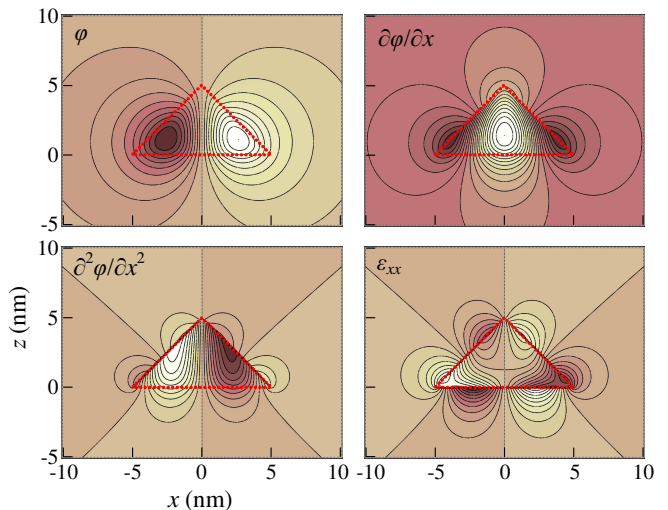


FIG. 9. Isoline plots (in the plane $y = 0$) of the potential φ , its derivatives $\partial\varphi/\partial x$, $\partial^2\varphi/\partial x^2$, and the strain component ε_{xx} produced by a pyramidal inclusion with height $h = 5$ nm and the length of the square base $l = 10$ nm. (See Fig. 8 for a sketch of the inclusion.) The eigenstrain $\varepsilon_0(\mathbf{r})$ inside the inclusion is approximately proportional to $\sin(kx)$ with $k = 2\pi/l$, see Eq. (101). Poisson ratio $\nu = 0.25$. The isolines are equidistant, brighter areas correspond to larger values. The inclusion cross section is shown by the red dotted contour.

Steps 8, 9, 11 of the algorithm only when index m , n or t becomes larger than 1, that occurs only if $N \geq 2$. Hence, to check the algorithm, it is necessary to consider at least quadratic ($N = 2$) coordinate dependence of the eigenstrain. In the example of this Subsection, N is equal to 9, that provides a good test of the algorithm as a whole.

IX. CONCLUDING REMARKS

Two problems, closely related to each other, are considered in this paper. The first one is the search for an analytical solution (in a closed form) for the spatial distribution of the elastic strain induced by a lattice-mismatched inclusion inserted in an infinite matrix, in the case of a polyhedral shape of the inclusion. The second problem is finding an analytical solution for an electrostatic or gravitational potential created by a polyhedral body, and for the derivatives of the potential. It is well known that the strain tensor is expressed via the second derivatives of the potential, see Eq. (12), assuming that the inclusion and the matrix are elastically isotropic and have the same elastic constants. Under these assumptions, we obtained the universal analytical expression describing the strain distribution, Eq. (82), for a polynomial coordinate dependence of the lattice misfit within the inclusion. Similar analytical formulas, Eqs. (83)–(85), were derived for the potential and its first and second derivatives in the case of a polynomial distribution of the charge/mass density over a polyhedral-

shaped body.

The results of the present work allow one to understand the structure of the known analytical solutions for different particular cases, e. g. strain distributions due to homogeneous polyhedral inclusions, potentials of polyhedral bodies with a constant density or a constant gradient of the density. Typically, the solutions found in the literature are combinations of logarithmic terms and terms containing inverse trigonometric functions, mostly arctangents. Our expressions (83)–(85) clarify that logarithmic terms arise from potentials of uniformly charged edges $L^{(k)}$, and arctangent terms—from solid angles $\Omega^{(i)}$.

Finally, it is worth highlighting several ways of generalizing the results of the present study. The strain distribution for an inclusion in a half-space can be found by the “mirror image” method.⁶⁸ The effects of anisotropy can be taken into account either by series expansion of the elastic Green’s function,^{69,70} or by the method of stretching the coordinates.^{16,36} In the case of different elastic constants of the matrix and the inclusion (an inhomogeneous inclusion), one can apply the perturbation method based on the concept of effective inclusion.^{71,72}

ACKNOWLEDGMENTS

This work is funded by RFBR (grants #16-29-14031 and #16-02-00397, development of analytical expressions) and by State Programme (Grant No. 0306-2016-0015, creating the computer program for calculation of the strain).

Appendix A: Integrals containing the derivatives of characteristic function $\chi(\mathbf{r})$

This Appendix is devoted to reducing the integrals $\varphi_{,\alpha}^{(mnp)}$ and $\varphi_{,\alpha\beta}^{(mnp)}$ defined by Eqs. (24) and (25) to the primitive introduced in Section IV.

Let us define a function $f(\mathbf{r})$ as

$$f(x, y, z) = (x - X)^m (y - Y)^n (z - Z)^p, \quad (\text{A1})$$

then

$$\varphi_{,\alpha}^{(mnp)} = \iiint \frac{\partial [f(\mathbf{r}) \chi(\mathbf{r})]}{\partial r_\alpha} \frac{d^3 r}{|\mathbf{r} - \mathbf{R}|} \quad (\text{A2})$$

and

$$\varphi_{,\alpha\beta}^{(mnp)} = \iiint \frac{\partial^2 [f(\mathbf{r}) \chi(\mathbf{r})]}{\partial r_\alpha \partial r_\beta} \frac{d^3 r}{|\mathbf{r} - \mathbf{R}|}. \quad (\text{A3})$$

First we will focus on the integral $\varphi_{,\alpha}^{(mnp)}$. Let us open the brackets in the expression $\partial(f\chi)/\partial r_\alpha$:

$$\frac{\partial(f\chi)}{\partial r_\alpha} = \frac{\partial f}{\partial r_\alpha} \chi + f \frac{\partial \chi}{\partial r_\alpha}. \quad (\text{A4})$$

Substituting this expansion into Eq. (A2), one can see that $\varphi_{,\alpha}^{(mnp)}$ is equal to the sum of two integrals, the first of which being the quantity $\varphi_{(mnp),\alpha}$ defined by Eq. (31). Therefore

$$\varphi_{,\alpha}^{(mnp)} = \varphi_{(mnp),\alpha} + \iiint f \frac{\partial \chi}{\partial r_\alpha} \frac{d^3 r}{|\mathbf{r} - \mathbf{R}|}. \quad (\text{A5})$$

In the remaining integral, the derivative $\partial\chi/\partial r_\alpha$ differs from zero only on the surface of the polyhedron; thus, it is in fact a surface integral. To be more precise, let us assume that the polyhedron is *convex* (generalization to non-convex polyhedra does not lead to any difficulties), and define the characteristic function $\chi(\mathbf{r})$ as follows:

$$\chi(\mathbf{r}) = \prod_{\substack{i \\ (\text{faces})}} \theta[\mathbf{n}_i \cdot (\mathbf{r}_i - \mathbf{r})], \quad (\text{A6})$$

where θ denotes the Heaviside step function, \mathbf{n}_i is the outward normal to i th face, and \mathbf{r}_i is a position vector of some (arbitrarily chosen) point on i th face. It is easy to check that Eqs. (5) and (A6) define the same function $\chi(\mathbf{r})$. Differentiation of each factor in Eq. (A6) is straightforward:

$$\frac{\partial}{\partial r_\alpha} \theta[\mathbf{n}_i \cdot (\mathbf{r}_i - \mathbf{r})] = -n_{i\alpha} \delta[\mathbf{n}_i \cdot (\mathbf{r}_i - \mathbf{r})], \quad (\text{A7})$$

where δ denotes the Dirac delta function. Using Eq. (A7), one can represent the derivative $\partial\chi/\partial r_\alpha$ as follows:

$$\frac{\partial \chi}{\partial r_\alpha} = - \sum_i n_{i\alpha} \psi_i(\mathbf{r}), \quad (\text{A8})$$

where functions ψ_i are defined as

$$\psi_i(\mathbf{r}) = \delta[\mathbf{n}_i \cdot (\mathbf{r}_i - \mathbf{r})] \prod_{j \neq i} \theta[\mathbf{n}_j \cdot (\mathbf{r}_j - \mathbf{r})]. \quad (\text{A9})$$

One can easily see that the function ψ_i vanishes everywhere except i th face of the polyhedron’s surface, where it has a δ -like singularity. Hence, any volume integral containing the function ψ_i is in fact a surface integral over i th face. In particular,

$$\iiint f \psi_i \frac{d^3 r}{|\mathbf{r} - \mathbf{R}|} = \iint_{\text{face } i} f \frac{dS}{|\mathbf{r} - \mathbf{R}|} = \Phi_{mnp}^{(i)}. \quad (\text{A10})$$

Using Eqs. (A8) and (A10), one can reduce the integral in the right-hand side of Eq. (A5) to surface integrals $\Phi_{mnp}^{(i)}$:

$$\iiint f \frac{\partial \chi}{\partial r_\alpha} \frac{d^3 r}{|\mathbf{r} - \mathbf{R}|} = - \sum_i n_{i\alpha} \Phi_{mnp}^{(i)}. \quad (\text{A11})$$

Substitution of this representation to Eq. (A5) gives rise to Eq. (30).

Hence, we have proved Eq. (30), i. e., have found out a representation of the integral $\varphi_{,\alpha}^{(mnp)}$ in terms of primitives.

Now let us consider the integral $\varphi_{,\alpha\beta}^{(mnp)}$. The second derivative in its definition, Eq. (A3), can be expanded as follows:

$$\frac{\partial^2(f\chi)}{\partial r_\alpha \partial r_\beta} = \frac{\partial^2 f}{\partial r_\alpha \partial r_\beta} \chi + \frac{\partial f}{\partial r_\beta} \frac{\partial \chi}{\partial r_\alpha} + \frac{\partial f}{\partial r_\alpha} \frac{\partial \chi}{\partial r_\beta} + f \frac{\partial^2 \chi}{\partial r_\alpha \partial r_\beta}. \quad (\text{A12})$$

After substituting this expansion to Eq. (A3), one gets four integrals corresponding to four terms of the right-hand side of Eq. (A12). The first integral is equal to the quantity $\varphi_{(mnp),\alpha\beta}$ introduced in Eq. (35):

$$\iiint \frac{\partial^2 f}{\partial r_\alpha \partial r_\beta} \chi \frac{d^3 r}{|\mathbf{r} - \mathbf{R}|} = \varphi_{(mnp),\alpha\beta}. \quad (\text{A13})$$

The second integral, which contains the derivative $\partial\chi/\partial r_\alpha$, can be treated as above, via Eqs. (A8) and (A10):

$$\begin{aligned} \iiint \frac{\partial f}{\partial r_\beta} \frac{\partial \chi}{\partial r_\alpha} \frac{d^3 r}{|\mathbf{r} - \mathbf{R}|} &= - \sum_i n_{i\alpha} \iiint \frac{\partial f}{\partial r_\beta} \psi_i \frac{d^3 r}{|\mathbf{r} - \mathbf{R}|} \\ &= - \sum_i n_{i\alpha} \iint_{\text{face } i} \frac{\partial f}{\partial r_\beta} \frac{dS}{|\mathbf{r} - \mathbf{R}|} = - \sum_i n_{i\alpha} \Phi_{(mnp),\beta}^{(i)}, \end{aligned} \quad (\text{A14})$$

where $\Phi_{(mnp),\beta}^{(i)}$ is the quantity defined by Eq. (36). The third integral is the same as the second one, up to the index permutation $\alpha \leftrightarrow \beta$. Therefore the expression for $\varphi_{,\alpha\beta}^{(mnp)}$ takes the following form:

$$\begin{aligned} \varphi_{,\alpha\beta}^{(mnp)} &= \varphi_{(mnp),\alpha\beta} - \sum_i n_{i\alpha} \Phi_{(mnp),\beta}^{(i)} - \sum_i n_{i\beta} \Phi_{(mnp),\alpha}^{(i)} \\ &\quad + \iiint f \frac{\partial^2 \chi}{\partial r_\alpha \partial r_\beta} \frac{d^3 r}{|\mathbf{r} - \mathbf{R}|}. \end{aligned} \quad (\text{A15})$$

In order to go further, one needs a method of dealing with integrals containing the second derivative $\partial^2\chi/\partial r_\alpha \partial r_\beta$. Using Eq. (A8), this second derivative can be represented as

$$\frac{\partial^2 \chi}{\partial r_\alpha \partial r_\beta} = - \sum_i n_{i\alpha} \frac{\partial \psi_i}{\partial r_\beta}. \quad (\text{A16})$$

Then, it is more convenient to define the function $\psi_i(\mathbf{r})$ in an alternative way:

$$\psi_i(\mathbf{r}) = \delta[\mathbf{n}_i \cdot (\mathbf{r}_i - \mathbf{r})] \prod_{\substack{k \\ (\text{edges})}} \theta[\mathbf{b}_{ik} \cdot (\mathbf{r}_k - \mathbf{r})], \quad (\text{A17})$$

where index k runs over the edges that surround i th face, and unit vectors \mathbf{b}_{ik} are directed out of i th face perpendicularly to their corresponding edges, as shown

in Fig. 2. One can easily figure out that both equations (A9) and (A17) define the same function, which has delta-function-like behaviour on i th face and is equal to zero outside this face. Consequently, the derivative $\partial\psi_i/\partial r_\beta$ takes the form

$$\frac{\partial \psi_i}{\partial r_\beta} = -n_{i\beta} \omega_i(\mathbf{r}) - \sum_k b_{ik\beta} \eta_k(\mathbf{r}), \quad (\text{A18})$$

where

$$\omega_i(\mathbf{r}) = \delta'[\mathbf{n}_i \cdot (\mathbf{r}_i - \mathbf{r})] \prod_k \theta[\mathbf{b}_{ik} \cdot (\mathbf{r}_k - \mathbf{r})] \quad (\text{A19})$$

and

$$\eta_k(\mathbf{r}) = \delta[\mathbf{n}_i \cdot (\mathbf{r}_i - \mathbf{r})] \delta[\mathbf{b}_{ik} \cdot (\mathbf{r}_k - \mathbf{r})] \prod_{k' \neq k} \theta[\mathbf{b}_{ik'} \cdot (\mathbf{r}_{k'} - \mathbf{r})]. \quad (\text{A20})$$

(Notably, the function $\eta_k(\mathbf{r})$ is one and the same for both faces adjacent to k th edge.) The term containing ω_i arises in Eq. (A18) from differentiating the delta-functional factor in Eq. (A17), and the terms with η_k —from differentiating Heaviside θ -functions in a manner similar to Eq. (A7). With Eqs. (A16) and (A18) one can represent second derivatives of χ as

$$\frac{\partial^2 \chi}{\partial r_\alpha \partial r_\beta} = \sum_i n_{i\alpha} n_{i\beta} \omega_i(\mathbf{r}) + \sum_i \sum_k n_{i\alpha} b_{ik\beta} \eta_k(\mathbf{r}), \quad (\text{A21})$$

where index i runs over all faces, and index k —over edges adjacent to face i . Changing the order of summations in the last sum, and introducing the tensor $\lambda_{\alpha\beta}^{(k)}$ in accordance with Eq. (33), one can rewrite this representation in a more convenient form:

$$\frac{\partial^2 \chi}{\partial r_\alpha \partial r_\beta} = \sum_i n_{i\alpha} n_{i\beta} \omega_i(\mathbf{r}) + \sum_k \lambda_{\alpha\beta}^{(k)} \eta_k(\mathbf{r}), \quad (\text{A22})$$

where index k runs over all edges of the polyhedron. Hence, the integral in the right-hand side of Eq. (A15) is a linear combination of similar integrals containing ω_i or η_k instead of $\partial^2\chi/\partial r_\alpha \partial r_\beta$.

Let us consider the integral with ω_i . For convenience, we temporarily assume that i th face is perpendicular to the coordinate axis z . Then, the function $\omega_i(\mathbf{r})$ can be expressed as

$$\omega_i(x, y, z) = \delta'(z_i - z) \tilde{\chi}_i(x, y), \quad (\text{A23})$$

where z_i is the value of z at i th face, and the function $\tilde{\chi}_i(x, y)$ defines the polygon of i th face: $\tilde{\chi}_i(x, y) = 1$ if the point (x, y, z_i) lies inside the face, otherwise $\tilde{\chi}_i(x, y) = 0$. Therefore one can represent the integral with ω_i as follows:

$$\begin{aligned} \iiint f \omega_i \frac{d^3 r}{|\mathbf{r} - \mathbf{R}|} &= \iint \tilde{\chi}_i(x, y) dx dy \int \delta'(z_i - z) \frac{f}{|\mathbf{r} - \mathbf{R}|} dz. \end{aligned} \quad (\text{A24})$$

The inner integral can be taken by parts,

$$\begin{aligned} \int \delta'(z_i - z) \frac{f}{|\mathbf{r} - \mathbf{R}|} dz &= \int \delta(z_i - z) \frac{\partial}{\partial z} \left(\frac{f}{|\mathbf{r} - \mathbf{R}|} \right) dz \\ &= \int \delta(z_i - z) \left(\frac{\partial f}{\partial z} - f \frac{z - Z}{|\mathbf{r} - \mathbf{R}|^2} \right) \frac{dz}{|\mathbf{r} - \mathbf{R}|}, \quad (\text{A25}) \end{aligned}$$

and substitution of Eq. (A25) into Eq. (A24) leads to the following result:

$$\begin{aligned} \iiint_{\text{face } i} f \omega_i \frac{d^3 r}{|\mathbf{r} - \mathbf{R}|} &= \iint \left(\frac{\partial f}{\partial z} - f \frac{z - Z}{|\mathbf{r} - \mathbf{R}|^2} \right) \frac{dS}{|\mathbf{r} - \mathbf{R}|} \\ &= \Phi_{(mnp),z}^{(i)} + \Omega_{mnp}^{(i)}, \quad (\text{A26}) \end{aligned}$$

where the quantity $\Phi_{(mnp),z}^{(i)}$ is defined in Eq. (36). Though Eq. (A26) was derived in a special coordinate frame, one can easily make it independent of the choice of the frame. For that, it is enough to rewrite the term $\Phi_{(mnp),z}^{(i)}$ as $n_{i\gamma} \Phi_{(mnp),\gamma}^{(i)}$, i. e., in the invariant manner:

$$\iiint f \omega_i \frac{d^3 r}{|\mathbf{r} - \mathbf{R}|} = n_{i\gamma} \Phi_{(mnp),\gamma}^{(i)} + \Omega_{mnp}^{(i)}. \quad (\text{A27})$$

In order to calculate a similar integral with η_k , we choose (temporarily) a coordinate frame with axis z along the vector \mathbf{n}_i , and axis x along the vector \mathbf{b}_{ik} , so that axis y is directed along k th edge. In this frame, the expression (A20) can be rewritten as

$$\eta_k(x, y, z) = \delta(z_k - z) \delta(x_k - x) \tilde{\chi}_k(y), \quad (\text{A28})$$

where x_k and z_k are coordinates of k th edge, and the function $\tilde{\chi}_k(y)$ is equal to 1 if the point (x_k, y, z_k) lies on the edge, otherwise $\tilde{\chi}_k(y) = 0$. Then it is obvious that

$$\iiint f \eta_k \frac{d^3 r}{|\mathbf{r} - \mathbf{R}|} = L_{mnp}^{(k)} \quad (\text{A29})$$

according to the definition of $L_{mnp}^{(k)}$, Eq. (29). Of course, this result is invariant with respect to choice of the coordinate frame.

Finally, the combination of equations (A22), (A27), (A29) provides the following result for the integral that appears in Eq. (A15):

$$\begin{aligned} &\iiint f \frac{\partial^2 \chi}{\partial r_\alpha \partial r_\beta} \frac{d^3 r}{|\mathbf{r} - \mathbf{R}|} \\ &= \sum_i n_{i\alpha} n_{i\beta} \left(n_{i\gamma} \Phi_{(mnp),\gamma}^{(i)} + \Omega_{mnp}^{(i)} \right) + \sum_k \lambda_{\alpha\beta}^{(k)} L_{mnp}^{(k)}. \quad (\text{A30}) \end{aligned}$$

Substituting this expression into Eq. (A15), one obtains Eq. (34), which represents the quantity $\varphi_{,\alpha\beta}^{(mnp)}$ in terms of primitives.

Hence, Eq. (34) is proven, as well as Eq. (30).

Appendix B: Reducing volume integrals to surface integrals

The aim of this Appendix consists in deriving Eq. (47). For simplicity, let us consider the case of

$$\mathbf{R} = 0, \quad (\text{B1})$$

that does not lead to any loss of generality. (In order to account for nonzero \mathbf{R} , one can make the substitution $\mathbf{r} \rightarrow \mathbf{r} - \mathbf{R}$.) Let us define a vector field $\mathbf{F}(\mathbf{r})$ as

$$\mathbf{F}(\mathbf{r}) = \frac{\mathbf{r}}{r} x^m y^n z^p, \quad (\text{B2})$$

and apply Gauss's theorem:

$$\iiint_{\text{inclusion}} (\nabla \cdot \mathbf{F}) dV = \sum_i \iint_{\text{face } i} \mathbf{F} \cdot \mathbf{n}_i dS. \quad (\text{B3})$$

The integrand in the left-hand side of Eq. (B3) is

$$\nabla \cdot \mathbf{F} = (m + n + p + 2) \frac{x^m y^n z^p}{r}. \quad (\text{B4})$$

Therefore the left-hand side of Eq. (B3) is equal to $(m + n + p + 2) \varphi_{mnp}$. The integrand in the right-hand side of Eq. (B3) is

$$\mathbf{F} \cdot \mathbf{n}_i = \mathbf{r} \cdot \mathbf{n}_i \frac{x^m y^n z^p}{r}. \quad (\text{B5})$$

At any point of i th face, the factor $\mathbf{r} \cdot \mathbf{n}_i$ has the same value

$$\mathbf{r} \cdot \mathbf{n}_i = h_i, \quad (\text{B6})$$

where the quantity h_i is defined in Eq. (44). Therefore this factor can be carried out of the integral, and the integral over i th face in Eq. (B3) becomes equal to $h_i \Phi_{mnp}^{(i)}$. Hence, Eq. (B3) takes the following form:

$$(m + n + p + 2) \varphi_{mnp} = \sum_i h_i \Phi_{mnp}^{(i)}, \quad (\text{B7})$$

that proves validity of Eq. (47).

Appendix C: Converting primitives $\hat{\Phi}_{mn0}^{(i)}$ to $\hat{\Omega}_{mn0}^{(i)}$

Here we will derive Eq. (55). In order to simplify notations, we omit the hats at $\hat{x}, \hat{y}, \hat{z}, \hat{r}$. Consider the two-dimensional vector field (G_x, G_y) whose components are defined as

$$G_x(x, y) = \frac{x^{m+1} y^n}{r}, \quad G_y(x, y) = \frac{x^m y^{n+1}}{r}, \quad (\text{C1})$$

and write down a two-dimensional version of Gauss's theorem in the plane of i th face:

$$\iint_{\text{face } i} \left(\frac{\partial G_x}{\partial x} + \frac{\partial G_y}{\partial y} \right) dS = \sum_k \int_{\text{edge } k} (G_x b_{ikx} + G_y b_{iky}) dl, \quad (\text{C2})$$

where summation is over the edges surrounding face i ; b_{ikx} and b_{iky} are components of the vector \mathbf{b}_{ik} in the “tilted” frame.

The integrand of the surface integral in Eq. (C2) can be rewritten as

$$\frac{\partial G_x}{\partial x} + \frac{\partial G_y}{\partial y} = (m+n+1) \frac{x^m y^n}{r} + \frac{x^m y^n z^2}{r^3}, \quad (\text{C3})$$

and, according to the definitions (49a) and (49b), the left-hand side of Eq. (C2) obtains the following form:

$$\begin{aligned} \iint_{\text{face } i} \left(\frac{\partial G_x}{\partial x} + \frac{\partial G_y}{\partial y} \right) dS &= (m+n+1) \hat{\Phi}_{mn0}^{(i)} - \hat{\Omega}_{mn1}^{(i)} \\ &= (m+n+1) \hat{\Phi}_{mn0}^{(i)} - h_i \hat{\Omega}_{mn0}^{(i)}. \quad (\text{C4}) \end{aligned}$$

On the other hand, the integrand of the line integral in Eq. (C2) is

$$G_x b_{ikx} + G_y b_{iky} = (\mathbf{r} \cdot \mathbf{b}_{ik}) \frac{x^m y^n}{r}. \quad (\text{C5})$$

The factor $\mathbf{r} \cdot \mathbf{b}_{ik}$ is constant along the edge k , and has the value

$$\mathbf{r} \cdot \mathbf{b}_{ik} = B_{ik} \quad (\text{C6})$$

due to Eq. (45). Thus,

$$\int_{\text{edge } k} (G_x b_{ikx} + G_y b_{iky}) dl = B_{ik} \int_{\text{edge } k} \frac{x^m y^n}{r} dl = B_{ik} \hat{L}_{mn0}^{(k)}. \quad (\text{C7})$$

Collecting together Eqs. (C2), (C4), and (C7), one can get the relation

$$(m+n+1) \hat{\Phi}_{mn0}^{(i)} - h_i \hat{\Omega}_{mn0}^{(i)} = \sum_k B_{ik} \hat{L}_{mn0}^{(k)}, \quad (\text{C8})$$

which is equivalent to Eq. (55).

Appendix D: Decreasing the index n at $\hat{\Omega}_{mn0}^{(i)}$

In this Appendix we will derive the recursive relation (56) that allows a step-by-step decrease of the index n at $\hat{\Omega}_{mn0}^{(i)}$. As in the previous Appendix, we omit the hats at $\hat{x}, \hat{y}, \hat{z}, \hat{r}$.

Let us make simple transformations of the quantity $h_i \hat{\Phi}_{mn0}^{(i)}$:

$$\begin{aligned} h_i \hat{\Phi}_{mn0}^{(i)} &= \hat{\Phi}_{mn1}^{(i)} = \iint \frac{x^m y^n z}{r} dS \\ &= \iint \frac{x^2 + y^2 + z^2}{r^2} \frac{x^m y^n z}{r} dS = \iint \frac{x^{m+2} y^n z}{r^3} dS \\ &\quad + \iint \frac{x^m y^{n+2} z}{r^3} dS + \iint \frac{x^m y^n z^3}{r^3} dS \\ &= -\hat{\Omega}_{m+2,n,0}^{(i)} - \hat{\Omega}_{m,n+2,0}^{(i)} - \hat{\Omega}_{mn2}^{(i)}. \quad (\text{D1}) \end{aligned}$$

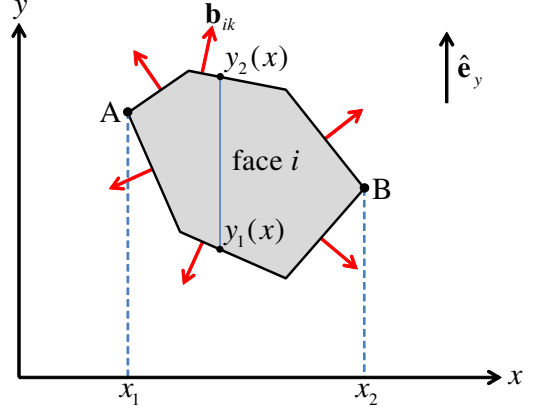


FIG. 10. How to evaluate the integral of $\hat{\Omega}_{m10}^{(i)}$.

(Integrals are over the i th face.) On the other hand, one can use Eq. (55) for reducing the value of $h_i \hat{\Phi}_{mn0}^{(i)}$ to quantities $\hat{\Omega}_{mn0}^{(i)}$ and $\hat{L}_{mn0}^{(k)}$:

$$h_i \hat{\Phi}_{mn0}^{(i)} = \frac{h_i^2}{m+n+1} \hat{\Omega}_{mn0}^{(i)} + \sum_k \frac{h_i B_{ik}}{m+n+1} \hat{L}_{mn0}^{(k)}, \quad (\text{D2})$$

where summation is over edges adjacent to face i . Since left-hand sides of Eqs. (D1) and (D2) are the same, then right-hand sides are equal to each other:

$$\begin{aligned} -\hat{\Omega}_{m+2,n,0}^{(i)} - \hat{\Omega}_{m,n+2,0}^{(i)} - \hat{\Omega}_{mn2}^{(i)} \\ = \frac{h_i^2}{m+n+1} \hat{\Omega}_{mn0}^{(i)} + \sum_k \frac{h_i B_{ik}}{m+n+1} \hat{L}_{mn0}^{(k)}. \quad (\text{D3}) \end{aligned}$$

Expressing $\hat{\Omega}_{m,n+2,0}^{(i)}$ from this equation, and taking into account that $\hat{\Omega}_{mn2}^{(i)} = h_i^2 \hat{\Omega}_{mn0}^{(i)}$ due to Eq. (53), one can get the following result:

$$\begin{aligned} \hat{\Omega}_{m,n+2,0}^{(i)} &= -\hat{\Omega}_{m+2,n,0}^{(i)} \\ &\quad - \frac{m+n+2}{m+n+1} h_i^2 \hat{\Omega}_{mn0}^{(i)} - \sum_k \frac{h_i B_{ik}}{m+n+1} \hat{L}_{mn0}^{(k)}. \quad (\text{D4}) \end{aligned}$$

Equation (56) can be obtained from Eq. (D4) by means of the substitution $n \rightarrow n-2$.

Appendix E: Reducing surface integrals $\hat{\Omega}_{m10}^{(i)}$ to line integrals

In this Appendix, we will derive Eq. (57) that simplifies the surface integral $\hat{\Omega}_{m10}^{(i)}$. As above, we will omit here the hats at $\hat{x}, \hat{y}, \hat{z}, \hat{r}$.

Let us perform integration of $\hat{\Omega}_{m10}^{(i)}$ over y :

$$\begin{aligned}\hat{\Omega}_{m10}^{(i)} &= - \iint_{\text{face } i} x^m y \frac{z}{r^3} dx dy = -h_i \int_{x_1}^{x_2} x^m dx \int_{y_1(x)}^{y_2(x)} \frac{y dy}{r^3} \\ &= h_i \int_{x_1}^{x_2} \frac{x^m dx}{r(x, y_2(x))} - h_i \int_{x_1}^{x_2} \frac{x^m dx}{r(x, y_1(x))}, \quad (\text{E1})\end{aligned}$$

where symbols x_1, x_2, y_1, y_2 are explained in Fig. 10; $r(x, y) = (x^2 + y^2 + h_i^2)^{1/2}$; h_i is z -coordinate of i th face. The first integral in the right-hand side of Eq. (E1) is taken over the upper part $y_2(x)$ of the periphery of i th face (between points A and B, see Fig. 10), and the second integral is over the lower part $y_1(x)$. It is convenient to express dx via the line element dl along the edge:

$$dx = \begin{cases} \mathbf{b}_{ik} \cdot \hat{\mathbf{e}}_y dl & \text{for upper part,} \\ -\mathbf{b}_{ik} \cdot \hat{\mathbf{e}}_y dl & \text{for lower part.} \end{cases} \quad (\text{E2})$$

By doing so, one can combine both integrals together, yielding

$$\hat{\Omega}_{m10}^{(i)} = h_i \sum_k \mathbf{b}_{ik} \cdot \hat{\mathbf{e}}_y \int_{\text{edge } k} \frac{x^m}{r} dl, \quad (\text{E3})$$

i. e.

$$\hat{\Omega}_{m10}^{(i)} = h_i \sum_k \mathbf{b}_{ik} \cdot \hat{\mathbf{e}}_y \hat{L}_{m00}^{(k)}. \quad (\text{E4})$$

Therefore we have obtained Eq. (57).

Appendix F: Decreasing the index m at $\hat{\Omega}_{m00}^{(i)}$

This Appendix is aimed to deduce the recursive rule (58) for reducing the index m at $\hat{\Omega}_{m00}^{(i)}$. As above, we will omit here the hats at $\hat{x}, \hat{y}, \hat{z}, \hat{r}$.

For this purpose, we rewrite the surface integral $\hat{\Omega}_{m20}^{(i)}$ in a manner similar to Eq. (E1):

$$\hat{\Omega}_{m20}^{(i)} = - \iint_{\text{face } i} x^m y^2 \frac{z}{r^3} dx dy = -h_i \int_{x_1}^{x_2} x^m dx \int_{y_1(x)}^{y_2(x)} \frac{y^2 dy}{r^3} \quad (\text{F1})$$

and make the integration by parts, taking into account that $y dy = d(r^2)/2$ and $d(y/r^3) = (1/r^3 - 3y^2/r^5)dy$:

$$\begin{aligned}\int_{y_1}^{y_2} \frac{y^2 dy}{r^3} &= \int_{y_1}^{y_2} \frac{y}{r^3} y dy = \frac{y}{r^3} \frac{r^2}{2} \Big|_{y_1}^{y_2} - \int_{y_1}^{y_2} \frac{r^2}{2} \left(\frac{1}{r^3} - \frac{3y^2}{r^5} \right) dy \\ &= \frac{y}{2r} \Big|_{y_1}^{y_2} - \frac{1}{2} \int_{y_1}^{y_2} \frac{dy}{r} + \frac{3}{2} \int_{y_1}^{y_2} \frac{y^2 dy}{r^3}, \quad (\text{F2})\end{aligned}$$

whence

$$\int_{y_1}^{y_2} \frac{y^2 dy}{r^3} = \int_{y_1}^{y_2} \frac{dy}{r} - \frac{y}{r} \Big|_{y_1}^{y_2}. \quad (\text{F3})$$

Substituting this into Eq. (F1), one can obtain

$$\begin{aligned}\hat{\Omega}_{m20}^{(i)} &= -h_i \int_{x_1}^{x_2} x^m dx \int_{y_1(x)}^{y_2(x)} \frac{dy}{r} \\ &+ h_i \int_{x_1}^{x_2} \frac{x^m y_2(x)}{r(x, y_2(x))} dx - h_i \int_{x_1}^{x_2} \frac{x^m y_1(x)}{r(x, y_1(x))} dx. \quad (\text{F4})\end{aligned}$$

The first term in the right hand side is equal to $-h_i \hat{\Phi}_{m00}^{(i)}$ (by definition of $\hat{\Phi}_{m00}^{(i)}$); the second and the third terms can be combined together, literally repeating the steps that lead from Eq. (E1) to Eq. (E4). This results in the following representation of $\hat{\Omega}_{m20}^{(i)}$:

$$\hat{\Omega}_{m20}^{(i)} = -h_i \hat{\Phi}_{m00}^{(i)} + h_i \sum_k (\mathbf{b}_{ik} \cdot \hat{\mathbf{e}}_y) L_{m10}^{(k)}, \quad (\text{F5})$$

where summation is over edges of i th face. The term $(-h_i \hat{\Phi}_{m00}^{(i)})$ can be reduced to Ω 's by means of Eq. (D1):

$$-h_i \hat{\Phi}_{m00}^{(i)} = \hat{\Omega}_{m+2,0,0}^{(i)} + \hat{\Omega}_{m20}^{(i)} + \hat{\Omega}_{m02}^{(i)}. \quad (\text{F6})$$

Substituting this into Eq. (F5), and expressing $\hat{\Omega}_{m02}^{(i)}$ as $h_i^2 \hat{\Omega}_{m00}^{(i)}$ according to Eq. (53), one can obtain the following relation:

$$\hat{\Omega}_{m+2,0,0}^{(i)} = -h_i^2 \hat{\Omega}_{m00}^{(i)} - h_i \sum_k (\mathbf{b}_{ik} \cdot \hat{\mathbf{e}}_y) L_{m10}^{(k)}, \quad (\text{F7})$$

from which one can get Eq. (58) by means of the substitution $m \rightarrow m - 2$.

Appendix G: Recursive formula for line integrals

Here we will obtain expressions (80), (81) for the integrals $\mathcal{L}_1^{(k)}, \mathcal{L}_2^{(k)}, \dots$. This can be done using integration by parts, taking into account that $\xi d\xi = \frac{1}{2} d(\rho_k^2 + \xi^2)$:

$$\begin{aligned}\mathcal{L}_t^{(k)} &= \int_{\xi_{k1}}^{\xi_{k2}} \frac{\xi^{t-1}}{\sqrt{\rho_k^2 + \xi^2}} \xi d\xi = \frac{\xi^{t-1}}{\sqrt{\rho_k^2 + \xi^2}} \frac{\rho_k^2 + \xi^2}{2} \Big|_{\xi_{k1}}^{\xi_{k2}} \\ &- \frac{1}{2} \int_{\xi_{k1}}^{\xi_{k2}} \frac{(t-1)\rho_k^2 \xi^{t-2} + (t-2)\xi^t}{\sqrt{\rho_k^2 + \xi^2}} d\xi. \quad (\text{G1})\end{aligned}$$

According to the definition (69), one can represent the last term as a combination of $\mathcal{L}_{t-2}^{(k)}$ and $\mathcal{L}_t^{(k)}$, yielding

$$\mathcal{L}_t^{(k)} = \frac{1}{2} \xi^{t-1} \sqrt{\rho_k^2 + \xi^2} \Big|_{\xi_{k1}}^{\xi_{k2}} - \frac{t-1}{2} \rho_k^2 \mathcal{L}_{t-2}^{(k)} - \frac{t-2}{2} \mathcal{L}_t^{(k)}, \quad (\text{G2})$$

whence

$$t\mathcal{L}_t^{(k)} + (t-1)\rho_k^2\mathcal{L}_{t-2}^{(k)} = \xi^{t-1}\sqrt{\rho_k^2 + \xi^2}\Big|_{\xi_{k1}}^{\xi_{k2}}. \quad (\text{G3})$$

Square roots $\sqrt{\rho_k^2 + \xi^2}$ at $\xi = \xi_{k1}, \xi_{k2}$ have the meaning of distances from the point \mathbf{R} to the ends of k th edge:

$$\sqrt{\rho_k^2 + \xi_{k1}^2} = \left| \mathbf{r}_A^{(k)} - \mathbf{R} \right|, \quad (\text{G4})$$

$$\sqrt{\rho_k^2 + \xi_{k2}^2} = \left| \mathbf{r}_B^{(k)} - \mathbf{R} \right|. \quad (\text{G5})$$

Therefore, Eq. (G3) takes the following form:

$$\begin{aligned} & t\mathcal{L}_t^{(k)} + (t-1)\rho_k^2\mathcal{L}_{t-2}^{(k)} \\ &= (\xi_{k2})^{t-1} \left| \mathbf{r}_B^{(k)} - \mathbf{R} \right| - (\xi_{k1})^{t-1} \left| \mathbf{r}_A^{(k)} - \mathbf{R} \right|, \quad (\text{G6}) \end{aligned}$$

Substituting ξ_{k1} and ξ_{k2} from Eq. (71) into Eq. (G6), and resolving the latter equation with respect to $\mathcal{L}_t^{(k)}$, one can get the recursive relation (80).

At $t = 1$, Eq. (G6) is simplified to

$$\mathcal{L}_1^{(k)} = \left| \mathbf{r}_B^{(k)} - \mathbf{R} \right| - \left| \mathbf{r}_A^{(k)} - \mathbf{R} \right|. \quad (\text{G7})$$

Appendix H: Comparison with a closed-form solution found in the literature

In order to check the validity of our analytical results, it is natural to compare them with similar results obtained by other authors. But it seems that there are no analytical calculations in the literature, related to polyhedral-shaped inclusions with a smoothly varied lattice misfit. For this reason, we choose as a “benchmark” the analytical results by Glas¹² for the strain distribution due to an inclusion having the shape of a truncated pyramid *with a constant misfit strain*. Such an analytical calculations can be found in Fig. 3b of Ref. 12.

In Fig. 11, we reproduce these calculations by our method—namely, by means of Eqs. (82) and (98). For the details of the inclusion geometry, see the caption to the figure. One can see that isolines in Fig. 11 are identical to ones in Fig. 3b of Ref. 12. That is, our method provides the same strain distribution as the closed-form analytical solution found by Glas¹² for the particular case of a truncated pyramid with a constant misfit strain.

Appendix I: Comparison with numerical calculations

The other useful test is comparison with numerical calculations. One difficulty in the way of such a comparison is that numerical methods deal with an elastic body of final size, whereas our analytical approach is valid for an inclusion in an infinitely large matrix. Therefore, in order to ensure that the analytical method and is compatible with numerical calculations, one should perform

numerical tests for different sizes of the matrix and check whether the strain distribution converges to the analytical solution when the matrix size grows.

An example of such a comparison is shown in Fig. 12. As a test sample, a pyramid-shaped inclusion with a linearly varying misfit strain is chosen. The parameters of the inclusion (see details in the caption to the figure) are taken the same as ones in Fig. 8. Therefore, the analytical solution in Fig. 12c is just the same as shown in Fig. 8. In order to obtain the numerical solutions, we used the COMSOL Multiphysics software. Simulations were performed by the finite-difference method for two different sizes of the “box”, which contains the pyramidal inclusion: $20 \times 20 \times 15$ nm (Fig. 12a) and $30 \times 30 \times 25$ nm (Fig. 12b), whereas the inclusion size is $10 \times 10 \times 5$ nm. One can see that, indeed, with increasing the size of the “box”, the strain distribution converges to the analytical solution.

It is worth to note that numerical results shown in Fig. 12a,b demanded about one hour of machine time on PC and about 20 gigabytes of memory, whereas the analytical calculation (Fig. 12c) lasts less than one minute and demands less than one megabyte of memory.

Appendix J: Pseudocode representation of the calculation algorithm

Calculation of the strain tensor $\varepsilon_{\alpha\beta}(\mathbf{r})$ for a set of points \mathbf{r} is a two-step procedure. The first step is the calculation of polynomials $\mathcal{A}_{\varepsilon\alpha\beta}^{(i)}$, $\mathcal{B}_{\varepsilon\alpha\beta}^{(k)}$, $\mathcal{C}_{\varepsilon\alpha\beta}^{(s)}$ for all faces, edges and vertices of the polyhedral inclusion, and for all values of tensor indices $\alpha\beta$. The second step is applying Eq. (82) for each point \mathbf{r} , that gives the value of $\varepsilon_{\alpha\beta}(\mathbf{r})$.

Below we represent these steps in a somewhat informal style, as Algorithm 1 and Algorithm 2, respectively. Algorithm 1 should be called six times—namely, for each pair xx, yy, zz, xy, xz and yz of the indices $\alpha\beta$. Then, Algorithm 2 is called as many times, as many points \mathbf{r} there are, at which the strain tensor $\varepsilon_{\alpha\beta}$ is to be calculated.

Algorithm 2 does not demand any further comments, since it simply calculates $\varepsilon_{\alpha\beta}$ via Eq. (82). But Algorithm 1 surely demands explanations. The idea of Algorithm 1 consists in the fact that, at each stage of the transformations described in Sections II–VI, the function $\varepsilon_{\alpha\beta}(\mathbf{R})$ is represented as a sum of contributions of such functions as $\varphi_{mnp}(\mathbf{R})$, $\Omega_{mnp}^{(i)}(\mathbf{R})$, etc., each of them being multiplied by some polynomial. Let us denote the polynomial corresponding to the function $\varphi_{mnp}(\mathbf{R})$ as $[\varphi_{mnp}]$, etc. Therefore,

$$\varepsilon_{\alpha\beta}(\mathbf{R}) = \sum_{m,n,p} [\varphi_{mnp}] \varphi_{mnp} + \sum_{i,m,n,p} [\Omega_{mnp}^{(i)}] \Omega_{mnp}^{(i)} + \dots$$

Then, let there be some identity connecting a function $A(\mathbf{R})$ with other functions $B(\mathbf{R})$, $C(\mathbf{R})$:

$$A(\mathbf{R}) = b(\mathbf{R}) B(\mathbf{R}) + c(\mathbf{R}) C(\mathbf{R}),$$

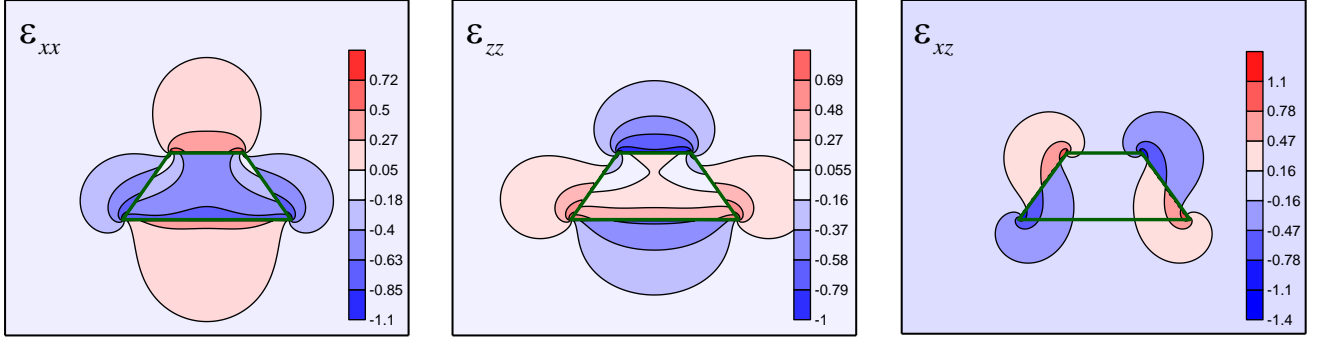


FIG. 11. Strain distribution due to an inclusion in the form of a truncated pyramid with a constant misfit strain. This strain distribution is calculated by our method described in Section VII, and one can see that it exactly reproduces the analytical calculations by Glas, see Fig. 3b in Ref. 12. Top and bottom faces of the truncated pyramid are squares lying in planes (001); four side faces have orientations $\{111\}$; the length of edges of the bottom face is 5 nm, and the height of the inclusion is equal to 2 nm. Poisson ratio $\nu = 1/3$. Strain components ε_{xx} , ε_{zz} and ε_{xz} are shown in the plane $y = 0$ (a plane of symmetry of the inclusion). The value of the strain is normalized by the misfit strain.

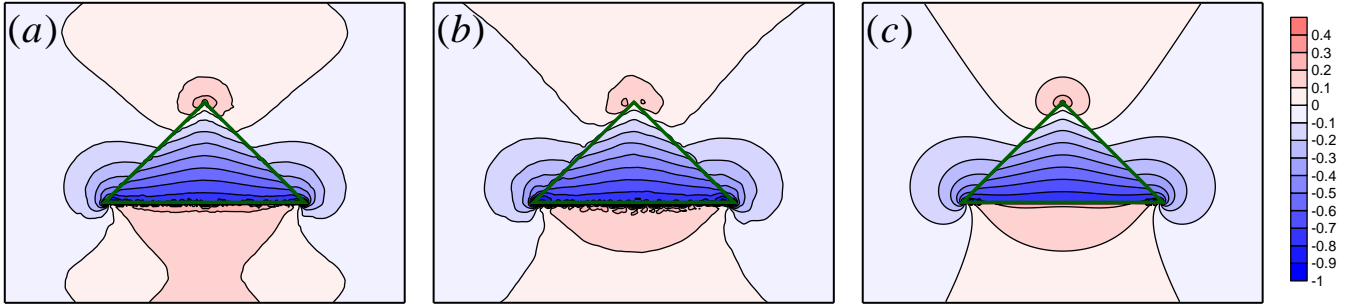


FIG. 12. Comparison between numerical and analytical results of the strain calculation. Shown is the distribution of the strain component ε_{xx} due to a pyramid-shaped inclusion with a misfit strain decreasing linearly from bottom to top: (a) numerical calculations with the box size $20 \times 20 \times 15$ nm; (b) numerical calculations with the box size $30 \times 30 \times 25$ nm; (c) analytical calculations assuming that the inclusion is incorporated in an infinite matrix. One can see that with increasing the box size the numerical results (a,b) converge to analytical ones (c). The geometry of the inclusion is the same as in Fig. 8: the pyramid base has orientation (001) and is a square with the side length $l = 10$ nm; the pyramid height is $h = 5$ nm; the misfit strain near the apex is twice smaller than that near the base. Poisson ratio $\nu = 0.25$. The component ε_{xx} is shown in the plane $y = 0$ (a plane of symmetry), the values of the strain are normalized by the misfit strain near the pyramid base. Numerical calculations (a,b) are performed by the finite-element method using the COMSOL Multiphysics software. Free boundary conditions are applied at the surface of the box. Analytical calculations (c) are made by the method of Section VII.

where $b(\mathbf{R})$, $c(\mathbf{R})$ are some polynomials. Then, one can rewrite the contribution $[A] A$ of the function A into $\varepsilon_{\alpha\beta}$ as

$$[A] A = ([A] b) B + ([A] c) C,$$

i. e. transform it into contributions of B and C . Such a transformation can be implemented in the algorithm as a transformation of polynomial $[A]$ into polynomials $[B]$, $[C]$ as follows:

- 1: $[B] = [A] b$
- 2: $[C] = [A] c$
- 3: $[A] = 0$

Implementing different identities from Sections II–VI in a due order, one can transform all the polynomials like $[\varphi_{mnp}]$, $[\Omega_{mnp}^{(i)}]$, etc. into the following ones: $[\Omega_{000}^{(i)}] \equiv \mathcal{A}_{\varepsilon\alpha\beta}^{(i)}$, $[L_{000}^{(k)}] \equiv \mathcal{B}_{\varepsilon\alpha\beta}^{(k)}$, and $[|\mathbf{R} - \mathbf{r}_s|] \equiv \mathcal{C}_{\varepsilon\alpha\beta}^{(s)}$ for different i, k, s . This is how one can find out the polynomials \mathcal{A} , \mathcal{B} , \mathcal{C} . This is the idea, on which Algorithm 1 is based.

It is important to note that Algorithm 1 is by no means optimized. Its performance and memory requirements can be easily improved, but we leave it here in its non-optimized version, in order to keep its form as close to equations of Sections II–VI as possible. The numbers of used equations are indicated in comments.

Algorithm 1: finding out the polynomials $\mathcal{A}_{\varepsilon\alpha\beta}^{(i)}$, $\mathcal{B}_{\varepsilon\alpha\beta}^{(k)}$, $\mathcal{C}_{\varepsilon\alpha\beta}^{(s)}$

Input:

tensor indices α, β determining which strain component $\varepsilon_{\alpha\beta}$ we are going to calculate;
 polynomial C , which defines the coordinate dependence of the eigenstrain within the inclusion;
 degree N of the polynomial C ;

the geometry of the polyhedral inclusion: coordinates of vertices; the set of unit vectors $\mathbf{n}_i, \mathbf{b}_{ik}, \mathbf{l}_k$ that describes orientations of faces and edges; for each face i (edge k), one arbitrarily chosen point \mathbf{r}_i (\mathbf{r}_k) on it;
 Poisson ratio ν .

Output: polynomials $\mathcal{A}_{\varepsilon\alpha\beta}^{(i)}$ for each face i , $\mathcal{B}_{\varepsilon\alpha\beta}^{(k)}$ for each edge k , $\mathcal{C}_{\varepsilon\alpha\beta}^{(s)}$ for each vertex s .

Variables:

integer numbers: $i, i_1, i_2, k, m, n, p, m', n', p', t, \gamma$;

real numbers, vectors and arrays: $\Lambda, \lambda_{\alpha\beta}^{(k)}, \hat{\mathbf{e}}_x, \hat{\mathbf{e}}_y, \hat{\mathbf{e}}_z, \mathbf{r}_A, \mathbf{r}_B, T_{mnp}^{m'n'p'}$;

polynomials (of degree N) and arrays of polynomials: $[\varphi_{m,n,p}]$, $[\Phi_{m,n,p}^{(i)}]$, $[\Omega_{m,n,p}^{(i)}]$, $[L_{m,n,p}^{(k)}]$, $[\hat{\Phi}_{m,n,p}^{(i)}]$, $[\hat{\Omega}_{m,n,p}^{(i)}]$, $[\hat{L}_{m,n,p}^{(k)}]$, $[\varphi_{\alpha\beta}^{(mnp)}]$, $[\varphi_{(mnp),\alpha\beta}]$, $[\Phi_{(mnp),\gamma}^{(i)}]$, $[\mathcal{L}_t^{(k)}]$, h_i , B_{ik} , $\mathbf{r}_0^{(k)}$, ρ_k^2 , \tilde{C}_{mnp} , P_A , P_B .

(Note 1: polynomials can be stored as real arrays $(N+1) \times (N+1) \times (N+1)$ of their coefficients.)

(Note 2: this algorithm can be modified for calculating the potential or its first derivatives, but in this case some polynomials will have degrees $N+2$ and $N+1$, respectively.)

```

1:                                                                                                     ▷ Initialization:
2: set polynomials  $\mathcal{A}_{\varepsilon\alpha\beta}^{(i)}$ ,  $\mathcal{B}_{\varepsilon\alpha\beta}^{(k)}$ ,  $\mathcal{C}_{\varepsilon\alpha\beta}^{(s)}$  to zero
3: for all  $m \geq 0, n \geq 0, p \geq 0$  ( $m+n+p \leq N$ ) do
4:    $[\varphi_{m,n,p}] = 0$ 
5:   for all faces  $i$  do
6:      $[\Phi_{m,n,p}^{(i)}] = 0$ 
7:   end for
8: end for
9: for  $t = 0$  to  $N$  do
10:  for all edges  $k$  do
11:     $[\mathcal{L}_t^{(k)}] = 0$ 
12:  end for
13: end for
14: for all faces  $i$  do
15:  define polynomial  $h_i$  as follows:  $h_i(\mathbf{R}) = (\mathbf{r}_i - \mathbf{R}) \cdot \mathbf{n}_i$                                      ▷ Eq. (44)
16:  for all edges  $k$  adjacent to face  $i$  do
17:    define polynomial  $B_{ik}$  as follows:  $B_{ik}(\mathbf{R}) = (\mathbf{r}_k - \mathbf{R}) \cdot \mathbf{b}_{ik}$                                      ▷ Eq. (45)
18:  end for
19: end for
20: for all edges  $k$  do
21:  define polynomials  $\mathbf{r}_0^{(k)} = \{x_0^{(k)}, y_0^{(k)}, z_0^{(k)}\}$  and  $\rho_k^2$  as follows:
22:   $\mathbf{r}_0^{(k)}(\mathbf{R}) = \mathbf{r}_k - \mathbf{l}_k[\mathbf{l}_k \cdot (\mathbf{r}_k - \mathbf{R})]$ ,                                                                                                     ▷ Eq. (73)
23:   $\rho_k^2(\mathbf{R}) = |\mathbf{r}_k - \mathbf{R}|^2 - [\mathbf{l}_k \cdot (\mathbf{r}_k - \mathbf{R})]^2$ .                                                                                                     ▷ Eq. (70)
24: end for
25:  $\Lambda = \frac{1}{4\pi} \frac{1+\nu}{1-\nu}$                                                                                                      ▷ Eq. (10)
26:
27:                                                                                                     ▷ Steps 1, 2:
28: for all  $m \geq 0, n \geq 0, p \geq 0$  ( $m+n+p \leq N$ ) do
29:  calculate polynomial  $\tilde{C}_{mnp}$  according to Eq. (19)
30:   $[\varphi_{\alpha\beta}^{(mnp)}] = -\Lambda \tilde{C}_{mnp}$                                                                                                      ▷ Eqs. (12), (22)
31: end for
32: for all faces  $i$  do
33:  add  $\frac{\delta_{\alpha\beta}}{4\pi} C$  to  $\mathcal{A}_{\varepsilon\alpha\beta}^{(i)}$                                                                                                      ▷ Eqs. (12), (42), (3)
34: end for
35:                                                                                                     ▷ Step 3:
36: for all  $m \geq 0, n \geq 0, p \geq 0$  ( $m+n+p \leq N$ ) do

```

```

37:    $[\varphi_{(mnp),\alpha\beta}] = [\varphi_{\alpha\beta}^{(mnp)}]$  ▷ begin of Eq. (34)
38:   for all faces  $i$  do
39:     for all  $\gamma \in \{x, y, z\}$  do
40:        $[\Phi_{(mnp),\gamma}^{(i)}] = (-n_{i\alpha}\delta_{\beta\gamma} - n_{i\beta}\delta_{\alpha\gamma} + n_{i\alpha}n_{i\beta}n_{i\gamma}) [\varphi_{\alpha\beta}^{(mnp)}]$ 
41:     end for
42:      $[\Omega_{m,n,p}^{(i)}] = n_{i\alpha}n_{i\beta} [\varphi_{\alpha\beta}^{(mnp)}]$ 
43:   end for
44:   for all edges  $k$  do
45:     find two faces  $i_1, i_2$  adjacent to edge  $k$ 
46:      $\lambda_{\alpha\beta}^{(k)} = n_{i_1\alpha}b_{i_1k\beta} + n_{i_2\alpha}b_{i_2k\beta}$  ▷ Eq. (33)
47:      $[L_{m,n,p}^{(k)}] = \lambda_{\alpha\beta}^{(k)} [\varphi_{\alpha\beta}^{(mnp)}]$ 
48:   end for
49:    $[\varphi_{\alpha\beta}^{(mnp)}] = 0$  ▷ end of Eq. (34)
50:   if  $(\alpha\beta) = (xx)$  and  $m \geq 2$  then ▷ begin of Eq. (37)
51:     add  $m(m-1) [\varphi_{(mnp),\alpha\beta}]$  to  $[\varphi_{m-2,n,p}]$ 
52:   else if  $(\alpha\beta) = (yy)$  and  $n \geq 2$  then
53:     add  $n(n-1) [\varphi_{(mnp),\alpha\beta}]$  to  $[\varphi_{m,n-2,p}]$ 
54:   else if  $(\alpha\beta) = (zz)$  and  $p \geq 2$  then
55:     add  $p(p-1) [\varphi_{(mnp),\alpha\beta}]$  to  $[\varphi_{m,n,p-2}]$ 
56:   else if  $(\alpha\beta) = (xy)$  or  $(yx)$  and  $m \geq 1$  and  $n \geq 1$  then
57:     add  $mn [\varphi_{(mnp),\alpha\beta}]$  to  $[\varphi_{m-1,n-1,p}]$ 
58:   else if  $(\alpha\beta) = (xz)$  or  $(zx)$  and  $m \geq 1$  and  $p \geq 1$  then
59:     add  $mp [\varphi_{(mnp),\alpha\beta}]$  to  $[\varphi_{m-1,n,p-1}]$ 
60:   else if  $(\alpha\beta) = (yz)$  or  $(zy)$  and  $n \geq 1$  and  $p \geq 1$  then
61:     add  $np [\varphi_{(mnp),\alpha\beta}]$  to  $[\varphi_{m,n-1,p-1}]$ 
62:   end if
63:    $[\varphi_{(mnp),\alpha\beta}] = 0$  ▷ end of Eq. (37)
64:   for all faces  $i$  do
65:     if  $m \geq 1$  then ▷ begin of Eq. (38)
66:       add  $m [\Phi_{(mnp),x}^{(i)}]$  to  $[\Phi_{m-1,n,p}^{(i)}]$ 
67:     end if
68:     if  $n \geq 1$  then
69:       add  $n [\Phi_{(mnp),y}^{(i)}]$  to  $[\Phi_{m,n-1,p}^{(i)}]$ 
70:     end if
71:     if  $p \geq 1$  then
72:       add  $p [\Phi_{(mnp),z}^{(i)}]$  to  $[\Phi_{m,n,p-1}^{(i)}]$ 
73:     end if
74:      $[\Phi_{(mnp),x}^{(i)}] = 0; [\Phi_{(mnp),y}^{(i)}] = 0; [\Phi_{(mnp),z}^{(i)}] = 0$  ▷ end of Eq. (38)
75:   end for
76: end for
77: ▷ Step 4:
78: for all  $m \geq 0, n \geq 0, p \geq 0$  ( $m+n+p \leq N$ ) do
79:   for all faces  $i$  do
80:     add  $\frac{1}{m+n+p+2} h_i [\varphi_{m,n,p}]$  to  $[\Phi_{m,n,p}^{(i)}]$  ▷ begin of Eq. (47)
81:   end for
82:    $[\varphi_{m,n,p}] = 0$  ▷ end of Eq. (47)
83: end for
84:
85: for all faces  $i$  do ▷ Now we are going to the tilted frame
86:
87:   for all  $m \geq 0, n \geq 0, p \geq 0$  ( $m+n+p \leq N$ ) do
88:      $[\hat{\Phi}_{m,n,p}^{(i)}] = 0$  ▷ Initialize polynomials related to the tilted frame
89:      $[\hat{\Omega}_{m,n,p}^{(i)}] = 0$ 
90:     for all edges  $k$  adjacent to face  $i$  do
91:        $[\hat{L}_{m,n,p}^{(k)}] = 0$ 

```

```

92:     end for
93: end for
94:
95: choose an orthonormal set of vectors  $\hat{\mathbf{e}}_x, \hat{\mathbf{e}}_y, \hat{\mathbf{e}}_z$  so that  $\hat{\mathbf{e}}_z = \mathbf{n}_i$  ▷ Step 5:
96: for all  $m \geq 0, n \geq 0, p \geq 0$  ( $m + n + p \leq N$ ) do
97:     for all  $m' \geq 0, n' \geq 0, p' \geq 0$  such that  $m' + n' + p' = m + n + p$  do
98:         calculate coefficient  $T_{mnp}^{m'n'p'}$  from Eq. (51)
99:         add  $T_{mnp}^{m'n'p'} [\Phi_{m,n,p}^{(i)}]$  to  $[\hat{\Phi}_{m',n',p'}^{(i)}]$  ▷ Eq. (50a)
100:        add  $T_{mnp}^{m'n'p'} [\Omega_{m,n,p}^{(i)}]$  to  $[\hat{\Omega}_{m',n',p'}^{(i)}]$  ▷ Eq. (50b)
101:    end for
102:     $[\Phi_{m,n,p}^{(i)}] = 0; [\Omega_{m,n,p}^{(i)}] = 0$  ▷ Eq. (50)
103: end for
104:
105: for all  $m \geq 0, n \geq 0, p \geq 1$  ( $m + n + p \leq N$ ) do ▷ Step 6:
106:     add  $(h_i)^p [\hat{\Phi}_{m,n,p}^{(i)}]$  to  $[\hat{\Phi}_{m,n,0}^{(i)}]; [\hat{\Phi}_{m,n,p}^{(i)}] = 0$  ▷ Eq. (53)
107:     add  $(h_i)^p [\hat{\Omega}_{m,n,p}^{(i)}]$  to  $[\hat{\Omega}_{m,n,0}^{(i)}]; [\hat{\Omega}_{m,n,p}^{(i)}] = 0$  ▷ Eq. (53)
108: end for
109:
110: for all  $m \geq 0, n \geq 0$  ( $m + n \leq N$ ) do ▷ Step 7:
111:     add  $\frac{h_i}{m+n+1} [\hat{\Phi}_{m,n,0}^{(i)}]$  to  $[\hat{\Omega}_{m,n,0}^{(i)}]$  ▷ begin of Eq. (55)
112:     for all edges  $k$  adjacent to face  $i$  do
113:         add  $\frac{B_{ik}}{m+n+1} [\hat{\Phi}_{m,n,0}^{(i)}]$  to  $[\hat{L}_{m,n,0}^{(k)}]$ 
114:     end for
115:      $[\hat{\Phi}_{m,n,0}^{(i)}] = 0$  ▷ end of Eq. (55)
116: end for
117:
118: if  $N \geq 2$  then ▷ Step 8:
119:     for  $m = 0$  to  $N - 2$  do
120:         for  $n = N - m$  down to 2 do
121:             add  $-\hat{\Omega}_{m,n,0}^{(i)}$  to  $[\hat{\Omega}_{m+2,n-2,0}^{(i)}]$  ▷ begin of Eq. (56)
122:             add  $-\frac{m+n}{m+n-1} (h_i)^2 [\hat{\Omega}_{m,n,0}^{(i)}]$  to  $[\hat{\Omega}_{m,n-2,0}^{(i)}]$ 
123:             for all edges  $k$  adjacent to face  $i$  do
124:                 add  $-\frac{h_i B_{ik}}{m+n-1} [\hat{\Omega}_{m,n,0}^{(i)}]$  to  $[\hat{L}_{m,n-2,0}^{(k)}]$ 
125:             end for
126:              $[\hat{\Omega}_{m,n,0}^{(i)}] = 0$  ▷ end of Eq. (56)
127:         end for
128:     end for
129: end if
130: if  $N \geq 1$  then
131:     for  $m = 0$  to  $N - 1$  do
132:         for all edges  $k$  adjacent to face  $i$  do
133:             add  $h_i (\mathbf{b}_{ik} \cdot \hat{\mathbf{e}}_y) [\hat{\Omega}_{m,1,0}^{(i)}]$  to  $[\hat{L}_{m,0,0}^{(k)}]$  ▷ begin of Eq. (57)
134:         end for
135:          $[\hat{\Omega}_{m,1,0}^{(i)}] = 0$  ▷ end of Eq. (57)
136:     end for
137: end if
138:
139: if  $N \geq 2$  then ▷ Step 9:
140:     for  $n = N$  down to 2 do
141:         add  $-(h_i)^2 [\hat{\Omega}_{m,0,0}^{(i)}]$  to  $[\hat{\Omega}_{m-2,0,0}^{(i)}]$  ▷ begin of Eq. (58)
142:         for all edges  $k$  adjacent to face  $i$  do
143:             add  $-h_i (\mathbf{b}_{ik} \cdot \hat{\mathbf{e}}_y) [\hat{\Omega}_{m,0,0}^{(i)}]$  to  $[\hat{L}_{m-2,1,0}^{(k)}]$ 
144:         end for
145:          $[\hat{\Omega}_{m,0,0}^{(i)}] = 0$  ▷ end of Eq. (58)
146:     end for
147: end if

```

```

148:   if  $N \geq 1$  then
149:       for all edges  $k$  adjacent to face  $i$  do
150:           add  $h_i(\mathbf{b}_{ik} \cdot \hat{\mathbf{e}}_x)$   $[\hat{\Omega}_{1,0,0}^{(i)}]$  to  $[\hat{L}_{0,0,0}^{(k)}]$  ▷ begin of Eq. (59)
151:       end for
152:        $[\hat{\Omega}_{1,0,0}^{(i)}] = 0$  ▷ end of Eq. (59)
153:   end if
154:   add  $[\hat{\Omega}_{0,0,0}^{(i)}]$  to  $\mathcal{A}_{\varepsilon\alpha\beta}^{(i)}$ ;  $[\hat{\Omega}_{0,0,0}^{(i)}] = 0$  ▷ (since  $\hat{\Omega}_{000}^{(i)} \equiv \Omega^{(i)}$ )
155:
156: ▷ Step 10 in the tilted frame:
157:   for all edges  $k$  adjacent to face  $i$  do
158:       for all  $m \geq 0, n \geq 0$  ( $m + n \leq N$ ) do
159:            $p = 0$ 
160:           for  $t = 0$  to  $m + n + p$  do
161:               calculate polynomial  $\hat{c}_{mnp,t}$  according to Eq. (78)
162:               add  $\hat{c}_{mnp,t}$   $[\hat{L}_{m,n,p}^{(k)}]$  to  $[\mathcal{L}_t^{(k)}]$  ▷ begin of Eq. (77)
163:           end for
164:            $[\hat{L}_{m,n,p}^{(k)}] = 0$  ▷ end of Eq. (77)
165:       end for
166:   end for
167:
168: end for ▷ Return back from the tilted frame
169:
170: ▷ Step 10 in the non-tilted frame:
171: for all edges  $k$  do
172:     for all  $m \geq 0, n \geq 0, p \geq 0$  ( $m + n + p \leq N$ ) do
173:         for  $t = 0$  to  $m + n + p$  do
174:             calculate polynomial  $c_{mnp,t}$  according to Eq. (75)
175:             add  $c_{mnp,t}$   $[L_{m,n,p}^{(k)}]$  to  $[\mathcal{L}_t^{(k)}]$  ▷ begin of Eq. (76)
176:         end for
177:          $[L_{m,n,p}^{(k)}] = 0$  ▷ end of Eq. (76)
178:     end for
179: end for
180:
181: ▷ Step 11:
182: for all edges  $k$  do
183:     Let A and B be numbers of the two vertices connected by edge  $k$ , and unit vector  $\mathbf{l}_k$  be directed from point
184:     A to point B. Let  $\mathbf{r}_A$  and  $\mathbf{r}_B$  be position vectors of these points.
185:     Define two polynomials  $P_A$  and  $P_B$  as follows:
186:      $P_A(\mathbf{R}) = \mathbf{l}_k \cdot (\mathbf{r}_A - \mathbf{R}), \quad P_B(\mathbf{R}) = \mathbf{l}_k \cdot (\mathbf{r}_B - \mathbf{R}).$ 
187:     if  $N \geq 2$  then
188:         for  $t = N$  down to 2 do
189:             add  $-\frac{t-1}{t}\rho_k^2$   $[\mathcal{L}_t^{(k)}]$  to  $[\mathcal{L}_{t-2}^{(k)}]$  ▷ begin of Eq. (80)
190:             add  $\frac{(P_B)^{t-1}}{t}$   $[\mathcal{L}_t^{(k)}]$  to  $\mathcal{C}_{\varepsilon\alpha\beta}^{(B)}$ 
191:             add  $-\frac{(P_A)^{t-1}}{t}$   $[\mathcal{L}_t^{(k)}]$  to  $\mathcal{C}_{\varepsilon\alpha\beta}^{(A)}$ 
192:              $[\mathcal{L}_t^{(k)}] = 0$  ▷ end of Eq. (80)
193:         end for
194:     end if
195:     if  $N \geq 1$  then
196:         add  $[\mathcal{L}_1^{(k)}]$  to  $\mathcal{C}_{\varepsilon\alpha\beta}^{(B)}$  ▷ begin of Eq. (81)
197:         add  $-[\mathcal{L}_1^{(k)}]$  to  $\mathcal{C}_{\varepsilon\alpha\beta}^{(A)}$ 
198:          $[\mathcal{L}_1^{(k)}] = 0$  ▷ end of Eq. (81)
199:     end if
200:     add  $[\mathcal{L}_0^{(k)}]$  to  $\mathcal{B}_{\varepsilon\alpha\beta}^{(k)}$ ;  $[\mathcal{L}_0^{(k)}] = 0$  ▷ (since  $\mathcal{L}_0^{(k)} \equiv L^{(k)}$ )
201: end for

```

Algorithm 2: calculating the strain tensor $\varepsilon_{\alpha\beta}(\mathbf{r})$ at one point \mathbf{r}

Input:

coordinates of the point \mathbf{r} where the strain tensor is to be calculated;
 coordinates of vertices of the polyhedral inclusion, connections between vertices, edges and faces of the polyhedron;
 the set of polynomials $\mathcal{A}_{\varepsilon\alpha\beta}^{(i)}$, $\mathcal{B}_{\varepsilon\alpha\beta}^{(k)}$, $\mathcal{C}_{\varepsilon\alpha\beta}^{(s)}$ for all faces, edges and vertices of the polyhedron (as calculated by Algorithm 1).

Output: the value of the strain tensor $\varepsilon_{\alpha\beta}$ at point \mathbf{r} .

Variables:

integer numbers: i, k, s, α, β ;

real numbers: $A, B, C, \Omega, L, R, l_A, l_B, l_{AB}$.

```

1: for  $\alpha \in \{x, y, z\}$  do
2:   for  $\beta \in \{x, y, z\}$  do
3:      $\varepsilon_{\alpha\beta} = 0$ 
4:   end for
5: end for
6:
7: for all faces  $i$  do ▷ the first sum in rhs of Eq. (82)
8:   Calculate the signed solid angle  $\Omega$  subtended by face  $i$  at point  $\mathbf{r}$ .
9:   (The sign of  $\Omega$  is positive (negative) when the outer (the inner) side of face  $i$  is seen from point  $\mathbf{r}$ .)
10:  ▷ Recipes for calculating solid angles can be found in Refs. 51 and 67.
11:  for all pairs  $\alpha\beta \in \{xx, yy, zz, xy, xz, yz\}$  do
12:     $A = \mathcal{A}_{\varepsilon\alpha\beta}^{(i)}(\mathbf{r})$  ▷ here we calculate the value of the polynomial function  $\mathcal{A}_{\varepsilon\alpha\beta}^{(i)}(x, y, z)$  at point  $\mathbf{r}$ 
13:     $\varepsilon_{\alpha\beta} = \varepsilon_{\alpha\beta} + A\Omega$ 
14:  end for
15: end for
16:
17: for all edges  $k$  do ▷ the second sum in rhs of Eq. (82)
18:   Let  $\mathbf{r}_A$  and  $\mathbf{r}_B$  be radius vectors of the two ends of edge  $k$ .
19:    $l_A = |\mathbf{r} - \mathbf{r}_A|$ ;  $l_B = |\mathbf{r} - \mathbf{r}_B|$ ;  $l_{AB} = |\mathbf{r}_A - \mathbf{r}_B|$ 
20:    $L = \log \frac{l_A + l_B + l_{AB}}{l_A + l_B - l_{AB}}$  ▷ Eq. (43)
21:   for all pairs  $\alpha\beta \in \{xx, yy, zz, xy, xz, yz\}$  do
22:      $B = \mathcal{B}_{\varepsilon\alpha\beta}^{(k)}(\mathbf{r})$ 
23:      $\varepsilon_{\alpha\beta} = \varepsilon_{\alpha\beta} + BL$ 
24:   end for
25: end for
26:
27: for all vertices  $s$  do ▷ the third sum in rhs of Eq. (82)
28:   Let  $\mathbf{r}_s$  be the radius vector of vertex  $s$ .
29:    $R = |\mathbf{r} - \mathbf{r}_s|$ ;
30:   for all pairs  $\alpha\beta \in \{xx, yy, zz, xy, xz, yz\}$  do
31:      $C = \mathcal{C}_{\varepsilon\alpha\beta}^{(s)}(\mathbf{r})$ 
32:      $\varepsilon_{\alpha\beta} = \varepsilon_{\alpha\beta} + CR$ 
33:   end for
34: end for
35:
36:  $\varepsilon_{yx} = \varepsilon_{xy}$ ;  $\varepsilon_{zx} = \varepsilon_{xz}$ ;  $\varepsilon_{zy} = \varepsilon_{yz}$ 

```

¹J. Stangl, V. Holý, and G. Bauer, Rev. Mod. Phys. **76**, 725 (2004).

²G. L. Bir and G. E. Pikus, *Symmetry and Strain-Induced Effects in Semiconductors* (Wiley, New York, 1974).

³C. G. Van de Walle, Phys. Rev. B **39**, 1871 (1989).

⁴A. V. Dvurechenskii, A. V. Nenashev, and A. I. Yakimov, Nan-

otechnology **13**, 75 (2002).

⁵A. F. Zinovieva, A. I. Nikiforov, V. A. Timofeev, A. V. Nenashev, A. V. Dvurechenskii, and L. V. Kulik, Phys. Rev. B **88**, 235308 (2013).

⁶M. Grundmann, O. Stier, and D. Bimberg, Phys. Rev. B **52**, 11969 (1995).

- ⁷C. Pryor, Phys. Rev. B **57**, 7190 (1998).
- ⁸O. Stier, M. Grundmann, and D. Bimberg, Phys. Rev. B **59**, 5688 (1999).
- ⁹V.-G. Stoleru, D. Pal, and E. Towe, Physica E: Low-dimensional Systems and Nanostructures **15**, 131 (2002).
- ¹⁰G. J. Rodin, Journal of the Mechanics and Physics of Solids **44**, 1977 (1996).
- ¹¹D. A. Faux, J. R. Downes, and E. P. O'Reilly, J. Appl. Phys. **82**, 3754 (1997).
- ¹²F. Glas, J. Appl. Phys. **90**, 3232 (2001).
- ¹³X. Jiang and E. Pan, International Journal of Solids and Structures **41**, 4361 (2004).
- ¹⁴W.-N. Zou, Q.-C. He, and Q.-S. Zheng, International Journal of Solids and Structures **48**, 2681 (2011).
- ¹⁵L. G. Sun, K. Y. Xu, and E. Pan, International Journal of Solids and Structures **49**, 1773 (2012).
- ¹⁶A. V. Nenashev, A. A. Koshkarev, and A. V. Dvurechenskii, Optoelectronics, Instrumentation and Data Processing **49**, 440 (2013).
- ¹⁷Q. D. Chen, K. Y. Xu, and E. Pan, International Journal of Solids and Structures **51**, 53 (2014).
- ¹⁸Y. M. Yue, K. Y. Xu, Q. D. Chen, and E. Pan, Acta Mechanica **226**, 2365 (2015).
- ¹⁹Y.-G. Lee, W.-N. Zou, and P. E., Proceedings Mathematical, Physical, and Engineering Sciences / The Royal Society **471**, 20140827 (2015).
- ²⁰J. D. Eshelby, Proceedings of the Royal Society of London A: Mathematical, Physical and Engineering Sciences **241**, 376 (1957).
- ²¹J. D. Eshelby, Proceedings of the Royal Society of London A: Mathematical, Physical and Engineering Sciences **252**, 561 (1959).
- ²²J. D. Eshelby, in *Progress in solid mechanics*, Vol. 2, edited by I. N. Sneddon and R. Hill (North-Holland, Amsterdam, 1961) pp. 89–140.
- ²³N. Kinoshita and T. Mura, physica status solidi (a) **5**, 759 (1971).
- ²⁴R. J. Asaro and D. M. Barnett, Journal of the Mechanics and Physics of Solids **23**, 77 (1975).
- ²⁵T. Mura and N. Kinoshita, physica status solidi (a) **48**, 447 (1978).
- ²⁶N. Kinoshita and T. Mura, Quarterly of Applied Mathematics **44**, 195 (1986).
- ²⁷H. Y. Yu, S. C. Sanday, and C. I. Chang, Proceedings of the Royal Society of London A: Mathematical, Physical and Engineering Sciences **444**, 239 (1994).
- ²⁸M. Rahman, Journal of Applied Mechanics **69**, 593 (2002).
- ²⁹Y. P. Chiu, Journal of Applied Mechanics **44**, 587 (1977).
- ³⁰Y. P. Chiu, Journal of Applied Mechanics **45**, 302 (1978).
- ³¹J. R. Downes, D. A. Faux, and E. P. O'Reilly, J. Appl. Phys. **81**, 6700 (1997).
- ³²G. S. Pearson and D. A. Faux, J. Appl. Phys. **88**, 730 (2000).
- ³³H. Nozaki and M. Taya, Journal of Applied Mechanics **68**, 441 (2000).
- ³⁴Q. Li and P. M. Anderson, Journal of elasticity and the physical science of solids **64**, 237 (2001).
- ³⁵I. A. Ovid'ko and A. G. Sheinerman, Reviews on Advanced Materials Science **9**, 17 (2005).
- ³⁶B. N. Kuvshinov, International Journal of Solids and Structures **45**, 1352 (2008).
- ³⁷A. V. Nenashev and A. V. Dvurechenskii, J. Appl. Phys. **107**, 064322 (2010).
- ³⁸X.-L. Gao and M. Liu, Journal of the Mechanics and Physics of Solids **60**, 261 (2012).
- ³⁹Z. Wang, H. Yu, and Q. Wang, International Journal of Plasticity **76**, 1 (2016).
- ⁴⁰P. Offermans, P. M. Koenraad, J. H. Wolter, K. Pierz, M. Roy, and P. A. Maksym, Phys. Rev. B **72**, 165332 (2005).
- ⁴¹M. Stoffel, A. Malachias, A. Rastelli, T. H. Metzger, and O. G. Schmidt, Appl. Phys. Lett. **94**, 253114 (2009).
- ⁴²A. Picco, E. Bonera, F. Pezzoli, E. Grilli, O. G. Schmidt, F. Isa, S. Cecchi, and M. Guzzi, Nanoscale Research Letters **7**, 1 (2012).
- ⁴³V. Pohánka, Geophysical Prospecting **46**, 391 (1998).
- ⁴⁴H. Holstein, Geophysics **68**, 157 (2003).
- ⁴⁵Hamayun, I. Prutkin, and R. Tenzer, Journal of Geodesy **83**, 1163 (2009).
- ⁴⁶M. G. D'Urso, Celestial Mechanics and Dynamical Astronomy **120**, 349 (2014).
- ⁴⁷J. T. Conway, Celestial Mechanics and Dynamical Astronomy **121**, 17 (2015).
- ⁴⁸D. Bhaskara Rao, M. J. Prakash, and N. Ramesh Babu, Geophysical Prospecting **38**, 411 (1990).
- ⁴⁹L. A. Gallardo-Delgado, M. A. Pérez-Flores, and E. Gómez-Treviño, Geophysics **68**, 949 (2003).
- ⁵⁰A. P. Gokula and R. G. Sastry, Journal of Earth System Science **124**, 1735 (2015).
- ⁵¹R. A. Werner and D. J. Scheeres, Celestial Mechanics and Dynamical Astronomy **65**, 313 (1996).
- ⁵²L. D. Landau and E. M. Lifshitz, *Theory of Elasticity* (Butterworth-Heinemann, Oxford, 1986).
- ⁵³J. H. Davies, J. Appl. Phys. **84**, 1358 (1998).
- ⁵⁴D. Nagy, Geophysics **31**, 362 (1966).
- ⁵⁵M. K. Paul, Pure and Applied Geophysics **112**, 553 (1974).
- ⁵⁶M. Okabe, Geophysics **44**, 730 (1979).
- ⁵⁷V. Pohánka, Geophysical Prospecting **36**, 733 (1988).
- ⁵⁸H. Holstein and B. Ketteridge, Geophysics **61**, 357 (1996).
- ⁵⁹H. Holstein, Geophysics **67**, 1126 (2002).
- ⁶⁰J. García-Abdeslem, Geophysics **70**, J39 (2005).
- ⁶¹M. G. D'Urso, Surveys in Geophysics **36**, 391 (2015).
- ⁶²R. A. Werner, Celestial Mechanics and Dynamical Astronomy **59**, 253 (1994).
- ⁶³R. A. Broucke, "Closed form expressions for some gravitational potentials," in *The Dynamics of Small Bodies in the Solar System: A Major Key to Solar Systems Studies*, edited by B. A. Steves and A. E. Roy (Springer Netherlands, Dordrecht, 1999) pp. 321–340.
- ⁶⁴I. E. Tamm, *Fundamentals of the Theory of Electricity* (Mir, Moscow, 1979).
- ⁶⁵J. A. Stratton, *Electromagnetic Theory* (McGraw-Hill, New York, 1941).
- ⁶⁶A. V. Oosterom and J. Strackee, IEEE Transactions on Biomedical Engineering **BME-30**, 125 (1983).
- ⁶⁷A. V. Nenashev and A. V. Dvurechenskii, "Strain distribution in quantum dot of arbitrary polyhedral shape: Analytical solution in closed form," (2007), arXiv:0707.2183.
- ⁶⁸J. H. Davies, Journal of Applied Mechanics **70**, 655 (2003).
- ⁶⁹D. A. Faux and G. S. Pearson, Phys. Rev. B **62**, R4798 (2000).
- ⁷⁰D. A. Faux and U. M. E. Christmas, J. Appl. Phys. **98**, 033534 (2005).
- ⁷¹H. Chu, E. Pan, J. Ramsey, J. Wang, and C. Xue, International Journal of Solids and Structures **48**, 673 (2011).
- ⁷²L. Ma and A. M. Korsunsky, International Journal of Solids and Structures **51**, 4477 (2014).